Influence of substrate composition and crystallographic orientation on the band structure of pseudomorphic Si-Ge alloy films

J. M. Hinckley and J. Singh
Center for High Frequency Microelectronics, Department of Electrical Engineering and Computer Science, The University of Michigan, Ann Arbor, Michigan 48109-2122
(Received 5 March 1990)

An analysis of the pseudomorphic $Si_{1-x}Ge_x$ band-structure variation with substrate composition and crystallographic orientation is reported. A method is presented for determining all six independent elements of the strain tensor in a strained epitaxial film grown on a substrate of arbitrary orientation. The substrate orientation is found to be an important factor in determining the band-structure properties of the epitaxial film. The strain-dependent band-structure properties investigated are the following: (1) The conduction band Γ_2', Δ_1, and L_1 valleys' shifts and degeneracy splittings, (2) the $k=0$ valence-band energy levels' shifts and degeneracy splittings, (3) the valence-band-state mixing, (4) the variation in the conduction- and valence-band-edge effective densities of state, (5) the variation in the intrinsic Fermi energy, and (6) the variation of the intrinsic-carrier concentration. It is shown that many aspects of the band structure—including the band gap, the density of states, and the position of the Δ_1-L_1 conduction-band-edge crossover—are each controllable through proper selection of film and substrate composition and crystallographic orientation.

I. INTRODUCTION

Currently, there is a great amount of research activity directed at extending heterostructure-device designs from binary-compound semiconductors to group-IV elemental or binary-alloy semiconductors involving $Si_{1-x}Ge_x$ alloy films. This work is motivated by the potential advantage of the superior performance of heterostructure devices achievable in the mature Si integrated-circuit technology. However, in contrast to many compound-semiconductor heterojunctions where lattice mismatch is slight for a significant band-gap difference (e.g., $GaAs/Al_xGa_{1-x}As$), the approximately 4% lattice mismatch between Si and Ge makes strain, due to lattice misfit, a major feature of $Si_{1-x}Ge_x$/Si heterostructures. When a film of $Si_{1-x}Ge_x$ is grown on a Si substrate, such strain may be expected to have an important effect on the band structure and, in turn, on the other electrical properties of the $Si_{1-x}Ge_x$ film. One of the primary effects of strain on the band structure is to lift various band-structure degeneracies through symmetry breaking. For example, in Si and high-Si-content Si-Ge alloys, the conduction-band edge is sixfold degenerate (six Δ_1 valleys), while the valence-band edge is twofold degenerate (heavy and light holes). Strain resulting from growth on a (001) substrate will lift the valence-band-edge degeneracy and reduce the conduction-band edge to either a twofold or a fourfold degeneracy for biaxial tensile or compressive strain, respectively. The design of optimum Si-Ge alloy heterostructure devices, will be determined, in part, by this effect of strain. Therefore, it becomes important to examine the effects of strain on the near-band-edge electronic properties of the Si-Ge alloy.

This paper describes some of the effects of lattice mismatch and substrate orientation on pseudomorphic $Si_{1-x}Ge_x$ films. Specifically, the near-band-edge band structure, the Fermi energy, the band-edge effective densities of state, and the intrinsic carrier concentration in the film are determined. All of these quantities are affected by strain in the film. The common configuration, currently utilized in both experimental and theoretical studies so far reported, is $Si_{1-x}Ge_x$/Si(001). Examples of these works may be found in the work by People[1] and the references cited therein. The strain tensor has a particularly simple form, and the effects of strain are well known in this configuration. However, a more general examination of the effects of strain can be made by allowing both the substrate lattice constant and orientation to vary, as in $Si_{1-x}Ge_x/Si_{1-y}Ge_y(hkl)$, thereby qualitatively varying the strain tensor. The objective of this work is to relate this type of substrate variation to changes in the properties of the alloy film listed above.

TABLE I. Si and Ge lattice material parameters.

Material parameter	Symbol	Si value	Refs.	Ge value	Refs.
lattice constant	a_0 (Å)	5.43095	2	5.6579	3
elastic stiffness	c_{11} (dyn cm^{-2})	16.56×10^{11}	4	12.853×10^{11}	4
	c_{12} (dyn cm^{-2})	6.39×10^{11}	4	4.826×10^{11}	4
	c_{44} (dyn cm^{-2})	7.95×10^{11}	4	6.680×10^{11}	4

TABLE II. Si and Ge conduction-band material parameters. m_0 is the electron rest mass.

Material parameter	Symbol	Si value	Refs.	Ge value	Refs.
conduction band	$E^{(000)}$ (eV)	4.0	5	0.805	6
	$E^{(100)}$ (eV)	1.110	7	0.86	8
	$E^{(111)}$ (eV)	1.65	9	0.645	8
direct band-gap pressure coefficient	$dE_g,d/dP$ (eV dyn^{-1} cm^2)			12.5×10^{-12}	10
indirect band-gap pressure coefficient	$dE_g,i/dP$ (eV dyn^{-1} cm^2)	-1.41×10^{-12}	7	5×10^{-12}	11
deformation potential	$\Xi_u^{(100)}$ (eV)	9.2	12		
	$\Xi_u^{(111)}$ (eV)			15.9	13
conduction-band effective mass	$m_d^{*(000)}/m_0$			0.038	14
	$m_d^{*(100)}/m_0$	0.357	15		
	$m_d^{*(111)}/m_0$			0.217	16

For the purpose of reference throughout the rest of this paper, the material parameters for Si and Ge which were used in the calculations in this work are tabulated in Tables I–III.[2–16] The corresponding parameters for the $Si_{1-x}Ge_x$ alloy will be given and discussed where first used, within the body of the paper.

Three different substrate crystallographic orientations are considered in this work: (001), (111), and (101). Furthermore, the degree and sense of lattice mismatch is varied by considering, for each of the three orientations, three substrate compositions: Si, Ge, and $Si_{0.5}Ge_{0.5}$. Both qualitative and quantitative changes are observed between films on these different substrates. Both Ge and $Si_{0.5}Ge_{0.5}$ (as well as other alloy compositions) could be effective substrates even though the starting substrate is Si, since by growth of a thick layer ($\sim$2–4 μm) of Ge or $Si_{0.5}Ge_{0.5}$ on Si, dislocations can, in principle, be generated and arrested with a free-standing epitaxial layer on which the strained film can be grown. This technique is used when GaAs-based devices are grown on Si substrates. For the purpose of this work, it is assumed that the strain in the epitaxial layer is coherent and that the in-plane lattice constant and symmetry of the strained layer are the same as those of the substrate.

The outline of the remainder of this paper is as follows. In Sec. II, the forms of the strain tensor and of Poisson's ratio are determined for epitaxial films grown on (001)-, (111)-, and (101)-oriented substrates. The development starts with the general form of Hooke's law and exploits the symmetry of each orientation. This derivation is given because, while the (001) substrate is commonly found in the literature, the other orientations have not been investigated, to our knowledge. A more general derivation, valid for an arbitrarily oriented substrate, which may not possess the rotational symmetry of the above orientations, is presented for completeness in the Appendix.

In Sec. III, the band structure and deformation-potential theory used in this work are described. The conduction band is characterized by three levels: Γ_2', Δ_1, and L_1. The valence band is characterized by the three levels of $\Gamma_8^- + \Gamma_6^-$. For a particular strain tensor, determined by the methods of Sec. II, the shifts and splittings of each of these levels is expressed in terms of deformation potentials. Also, the nature of the band-edge eigenstates is discussed in this section. These are of relevance in studies of both charge-carrier transport and polarization-dependent optical interactions, where transitions are governed by eigenstate-dependent selection rules.

In Sec. IV, the methods of calculating the intrinsic Fermi energy E_i the intrinsic carrier concentration n_i, and the conduction- and valence-band-edge effective densities of state N_c and N_v are presented. E_i and n_i are simultaneously determined such that charge neutrality is maintained. N_c and N_v are then determined from n_i, E_i, and

TABLE III. Si and Ge valence-band material parameters.

Material parameter	Symbol	Si value	Refs.	Ge value	Refs.
spin-orbit splitting	Δ_0 (eV)	0.044	17	0.282	18
valence band	L (dimensionless)	-5.78	19	-30.35	19
	M (dimensionless)	-3.44	19	-4.85	19
	N (dimensionless)	-8.64	19	-34.14	19
deformation potential	a (eV)	2.1	20	2.0	20
	b (eV)	-1.5	20	-2.2	20
	d (eV)	-3.4	20	-4.4	20

the band gap E_g.

Section V shows, in graphical form, the band shifts in strained $Si_{1-x}Ge_x$ as a function of x for each of the three substrate orientations [(001), (111), and (101)] and three substrate compositions (Si, Ge, and $Si_{0.5}Ge_{0.5}$). Also, for each of these nine substrates, n_i, N_c, and N_v are plotted as functions of film composition x. Considering a minimum useful critical thickness to be in the range of 100–500 Å, corresponding to approximately 2% lattice mismatch on Si(001),[1] serves as a guide to the useful range of x, depending on substrate composition. This range is, for Si substrates, $0.0 \le x \le 0.4$; for Ge substrates, $0.6 \le x \le 1.0$; and for $Si_{0.5}Ge_{0.5}$ substrates, $0.0 \le x \le 1.0$. These choices, although to some degree arbitrary, focus on what are likely to be the most useful alloy compositions for each given substrate.

Conclusions are presented in Sec. VI. As mentioned above, an appendix is included in which a derivation is presented for the strain tensor in a pseudomorphic film grown on an arbitrarily oriented substrate of the cubic crystal class O_h ($m3m$).

II. STRAIN TENSOR

An epitaxial film, which is not lattice matched to its substrate, will be under uniform biaxial contraction ($\varepsilon_{\parallel} < 0$) or dilation ($\varepsilon_{\parallel} > 0$), in the plane of the film. The in-plane strain $\varepsilon_{\parallel}$ is given by the substrate and layer material bulk lattice constants a_S and a_L, respectively:

$$\varepsilon_{\parallel} = \frac{a_S}{a_L} - 1 \ . \tag{1}$$

The substrate is assumed infinitely thick, so as to retain its bulk lattice spacing. There is no in-plane shear strain in the film, under uniform biaxial distortion (in-plane angles between ions are preserved).

Analysis of the system begins by adopting a coordinate system (x',y',z') in which the z' axis is normal to the substrate surface, and which is related to the coordinate system (x,y,z) of the primary crystallographic axes of the substrate by a rotation $\underline{U}$:

$$\underline{U} = \begin{bmatrix} \cos\varphi\cos\theta & -\sin\varphi & \cos\varphi\sin\theta \\ \sin\varphi\cos\theta & \cos\varphi & \sin\varphi\sin\theta \\ -\sin\theta & 0 & \cos\theta \end{bmatrix} . \tag{2}$$

The angles θ and φ are the polar and azimuthal angles of $\hat{\mathbf{z}}'$ relative to the coordinate system (x,y,z). The relation between coordinate systems for vectors and tensors is expressed as

$$\begin{aligned} r'_\alpha &= U_{\beta\alpha} r_\beta \ , \\ \varepsilon'_{\alpha\beta} &= U_{i\alpha} U_{j\beta} \varepsilon_{ij} \ , \\ C'_{\gamma\delta kl} &= U_{\alpha\gamma} U_{\beta\delta} U_{ik} U_{jl} C_{\alpha\beta ij} \ , \end{aligned} \tag{3}$$

where summation over repeated indices is indicated.

The in-plane strain tensor components are known to be $\varepsilon'_{11} = \varepsilon'_{22} = \varepsilon_{\parallel}$ (biaxial dilation or contraction), and $\varepsilon'_{12} = 0$ (no in-plane shear). The other three independent strain tensor elements $(\varepsilon'_{13}, \varepsilon'_{23}, \varepsilon'_{33})$ remain to be determined. The substrate applies a uniform in-plane stress to the film. This is the only external stress applied to the film. Thus $T'_{33} = T'_{23} = T'_{13} = 0$. T'_{11}, T'_{22}, and T'_{12} remain to be determined. Finally, the stress and strain tensor components are related by Hooke's law (within the linear elastic domain):

$$T'_{\alpha\beta} + C'_{\alpha\beta ij} \varepsilon'_{ij} = 0 \ , \tag{4}$$

for $\alpha,\beta = 1,2,3$. Summation over i and j is indicated. For $(\alpha\beta) = (33)$, (23), and (13), $T'_{\alpha\beta} = 0$, as above, and Hooke's law gives

$$\begin{aligned} C'_{33ij} \varepsilon'_{ij} &= 0 \ , \\ C'_{23ij} \varepsilon'_{ij} &= 0 \ , \\ C'_{13ij} \varepsilon'_{ij} &= 0 \ , \end{aligned} \tag{5}$$

where summation over repeated indices is indicated.

Up to this point, the discussion is perfectly general and applicable to cases of substrates of any arbitrary orientation. Now we will make the discussion more specific. In particular, only those substrates whose orientation is (001), (111), or (101) will be considered in what follows. These are distinguished from all other orientations by the fact that their normal is an axis of n-fold rotational symmetry ($n \ge 2$). This is important, as it allows a great simplification of the determination of the strain tensor. For cases of any other substrate orientation, the derivation is continued from this point in the Appendix.

Assuming that the substrate possesses n-fold ($n \ge 2$) rotational symmetry about its normal, the epitaxial film must also adopt this symmetry. The important result of this is that $\varepsilon'_{13} = \varepsilon'_{23} = 0$. This renders the system of Eqs. (5) redundant, any one of them being sufficient to determine the only remaining unknown strain tensor component ε'_{33}. Arbitrarily choosing to solve the first of these for ε'_{33},

$$\begin{aligned} \varepsilon'_{33} &= -\frac{C'_{3311}\varepsilon'_{11} + C'_{3322}\varepsilon'_{22}}{C'_{3333}} \\ &= -\left[\frac{C'_{3311} + C'_{3322}}{C'_{3333}}\right]\varepsilon_{\parallel} \ . \end{aligned} \tag{6}$$

Since Poisson's ratio σ is defined as $\varepsilon_{\parallel} = -\sigma\varepsilon'_{33}$, σ is found to be

$$\sigma = \frac{C'_{3333}}{C'_{3311} + C'_{3322}} \ . \tag{7}$$

To reiterate, $\varepsilon'_{11} = \varepsilon'_{22} = \varepsilon_{\parallel}$, $\varepsilon'_{33} = -\varepsilon_{\parallel}/\sigma$, and $\varepsilon'_{12} = \varepsilon'_{23} = \varepsilon'_{31} = 0$.

Now it remains only to determine $C'_{\alpha\beta ij}$ from $C_{\delta\gamma kl}$, to evaluate σ, and to determine ε_{ij} from ε'_{kl}. As stated earlier, the transformation between the coordinate systems [Eq. (2)] will depend upon the specific substrate orientation in question. The required elastic stiffness tensor elements C'_{33kk} are obtained:

$$C'_{33kk} = \sum_{\alpha,\beta,i,j=1}^{3} U_{\alpha 3} U_{\beta 3} U_{ik} U_{jk} C_{\alpha\beta ij} \ , \tag{8}$$

for $k=1,2,3$. This may be expanded and simplified by applying trigonometric identities to the components of $\underline{U}$. Furthermore, the elastic stiffness tensor of a material in the O_h ($m3m$) crystal class, such as Si or Ge, has only three distinct components, which are c_{11}, c_{12}, and c_{44}, in standard contracted index notation. The concluding result of the required algebraic manipulation is

$$\sigma=\frac{N}{D}\ , \tag{9}$$

$$N=C'_{3333}$$
$$=(c_{12}+2c_{44})+(c_{11}-c_{12}-2c_{44})(U_{13}^4+U_{23}^4+U_{33}^4)\ , \tag{10}$$

$$D=C'_{3311}+C'_{3322}$$
$$=(c_{11}+c_{12})-(c_{11}-c_{12})(U_{13}^4+U_{23}^4+U_{33}^4)$$
$$+4c_{44}[U_{13}U_{23}(U_{11}U_{21}+U_{12}U_{22})$$
$$+U_{13}U_{33}(U_{11}U_{31}+U_{12}U_{32})$$
$$+U_{23}U_{33}(U_{21}U_{31}+U_{22}U_{32})]\ . \tag{11}$$

For the (001) substrate, evaluations of N and D are trivial, since U is the identity matrix, (x,y,z) being coincident with (x',y',z'). With $U_{ij}=\delta_{ij}$, N and D are determined to be $N=c_{11}$ and $D=2c_{12}$, yielding the familiar $\sigma^{(001)}=\frac{1}{2}c_{11}/c_{12}$. For the second case, of the (111) substrate, $\underline{U}$ takes the form

$$\underline{U}^{(111)}=\begin{bmatrix}\frac{1}{\sqrt{6}} & \frac{-1}{\sqrt{2}} & \frac{1}{\sqrt{3}}\\ \frac{1}{\sqrt{6}} & \frac{1}{\sqrt{2}} & \frac{1}{\sqrt{3}}\\ \sqrt{\frac{2}{3}} & 0 & \frac{1}{\sqrt{3}}\end{bmatrix}\ . \tag{12}$$

From this, it follows that

$$N^{(111)}=\tfrac{1}{3}c_{11}+\tfrac{2}{3}c_{12}+\tfrac{4}{3}c_{44}\ ,$$
$$D^{(111)}=\tfrac{2}{3}c_{11}+\tfrac{4}{3}c_{12}-\tfrac{4}{3}c_{44}\ , \tag{13}$$

and

$$\sigma^{(111)}=\frac{c_{11}+2c_{12}+4c_{44}}{2c_{11}+4c_{12}-4c_{44}}\ . \tag{14}$$

For the third case, of the (101) substrate, $\underline{U}$ takes the form

$$\underline{U}^{(101)}=\begin{bmatrix}0 & \frac{-1}{\sqrt{2}} & \frac{1}{\sqrt{2}}\\ 0 & \frac{1}{\sqrt{2}} & \frac{1}{\sqrt{2}}\\ -1 & 0 & 0\end{bmatrix}\ . \tag{15}$$

From this, it follows as before that

$$N^{(101)}=\tfrac{1}{2}c_{11}+\tfrac{1}{2}c_{12}+c_{44}\ ,$$
$$D^{(101)}=\tfrac{1}{2}c_{11}+\tfrac{3}{2}c_{12}-c_{44}\ , \tag{16}$$

TABLE IV. Poisson's ratio σ for epitaxial films on (001), (111), and (101) substrates.

	$\sigma^{(001)}$	$\sigma^{(111)}$	$\sigma^{(101)}$
Si	1.296	2.275	1.959
Ge	1.332	2.691	2.222

and

$$\sigma^{(101)}=\frac{c_{11}+c_{12}+2c_{44}}{c_{11}+3c_{12}-2c_{44}}\ . \tag{17}$$

The determination of ε_{ij} from ε'_{kl}, as per Eq. (3), is obtained from

$$\varepsilon_{ij}=U_{ik}U_{jl}\varepsilon'_{kl}\ , \tag{18}$$

with summation over repeated indices. Using the $\underline{U}$ matrices given above, the strain tensors are as follows. For the (001) substrate,

$$\varepsilon_{xx}=\varepsilon_{yy}=\varepsilon_{\parallel}\ ,$$
$$\varepsilon_{zz}=-\varepsilon_{\parallel}/\sigma^{(001)}\ , \tag{19}$$
$$\varepsilon_{xy}=\varepsilon_{yz}=\varepsilon_{zx}=0\ .$$

For the (111) substrate,

$$\varepsilon_{xx}=\varepsilon_{yy}=\varepsilon_{zz}=\tfrac{1}{3}(2-1/\sigma^{(111)})\varepsilon_{\parallel}\ ,$$
$$\varepsilon_{xy}=\varepsilon_{yz}=\varepsilon_{zx}=-\tfrac{1}{3}(1+1/\sigma^{(111)})\varepsilon_{\parallel}\ . \tag{20}$$

For the (101) substrate,

$$\varepsilon_{xx}=\varepsilon_{zz}=\tfrac{1}{2}(1-1/\sigma^{(101)})\varepsilon_{\parallel}\ ,$$
$$\varepsilon_{yy}=\varepsilon_{\parallel}\ ,$$
$$\varepsilon_{xy}=-\tfrac{1}{2}(1+1/\sigma^{(101)})\varepsilon_{\parallel}\ , \tag{21}$$
$$\varepsilon_{yz}=\varepsilon_{zx}=0\ .$$

The values of $\sigma^{(001)}$, $\sigma^{(111)}$, and $\sigma^{(101)}$ for Si and Ge are shown in Table IV.

As stated earlier, strain in other substrate orientations is not analyzable by the same procedure since ε'_{13} and ε'_{23} may not be zero. A more general procedure, involving the simultaneous solution of the system of equations [Eq. (5)], is required. This procedure is outlined in the Appendix.

III. BAND STRUCTURE

The conduction band of materials in the unstrained, bulk $Si_{1-x}Ge_x$ is modeled as consisting of a Γ'_2 level with a spherical energy surface, a sixfold-degenerate Δ_1 level with ellipsoidal energy surfaces, and a fourfold-degenerate L_1 level, also with ellipsoidal energy surfaces. In Si, the direct band gap is too large to be important to the quantities of interest in this work. However, its value is retained from the literature in order to determine the position of the Γ'_2 level in high-Ge-content $Si_{1-x}Ge_x$ in which this level rises approximately linearly from its Ge

value, toward its Si value as x is decreased. The positions of the Γ_2', Δ_1, and L_1 levels for the bulk, unstrained alloy were obtained from the literature[5,8] and are given in Table V. The density-of-states effective mass for the Γ_2' and L_1 energy levels in $Si_{1-x}Ge_x$ are taken to be equal to their respective values in Ge, while the density-of-states effective mass for the Δ_1 energy level in $Si_{1-x}Ge_x$ is taken to be equal to its value in Si. This is a reasonable approximation, since it is supported, to within experimental error, by observation.[16,21]

The valence-band structure used in this work is calculated using a three-valence-band $\mathbf{k}\cdot\mathbf{p}$ method. The valence-band eigenstates in this method are formed from the six-dimensional basis for the $\Gamma_8^- + \Gamma_6^-$ representation: $|x\uparrow\rangle$, $|y\uparrow\rangle$, $|z\uparrow\rangle$, $|x\downarrow\rangle$, $|y\downarrow\rangle$, and $|z\downarrow\rangle$. The notation x,y,z refers to basis functions with the corresponding rotational symmetry of the Γ_{25}' representation of the symmetry group of the top of the valence band. The up and down arrows denote spin up ($+z$) and down ($-z$), respectively. As reported by Dresselhaus, Kip, and Kittel,[22] the $\mathbf{k}\cdot\mathbf{p}$ Hamiltonian matrix, in this basis, appropriate near the top of the valence band, is

$$\underline{H}_{\mathbf{k}\cdot\mathbf{p}} = \begin{bmatrix} \underline{H}' & \underline{0}_{3\times3} \\ \underline{0}_{3\times3} & \underline{H}' \end{bmatrix} \begin{matrix} \uparrow \\ \downarrow \end{matrix},$$

$$\underline{H}' = \frac{\hbar^2}{m} \begin{bmatrix} Lk_x^2 + M(k_y^2+k_z^2) & Nk_xk_y & Nk_zk_x \\ Nk_xk_y & Lk_y^2 + M(k_z^2+k_x^2) & Nk_yk_z \\ Nk_zk_x & Nk_yk_z & Lk_z^2 + M(k_x^2+k_y^2) \end{bmatrix} \begin{matrix} x \\ y \\ z \end{matrix}, \tag{22}$$

where m is the free-electron mass. The effect of the conduction band is implicitly contained in the dimensionless terms L, M, and N.

In contrast to the conduction band, spin-orbit coupling has a significant effect on the near-band-edge structure of the valence band. In the present work, the spin-orbit interaction is included by adding a wave-vector-independent perturbation matrix $\underline{H}_{\text{s.o.}}$ to $\underline{H}_{\mathbf{k}\cdot\mathbf{p}}$. In the above basis, $\underline{H}_{\text{s.o.}}$ is[23]

$$\underline{H}_{\text{s.o.}} = \frac{\Delta_0}{3} \begin{bmatrix} 0 & -i & 0 & 0 & 0 & 1 \\ i & 0 & 0 & 0 & 0 & -i \\ 0 & 0 & 0 & -1 & i & 0 \\ 0 & 0 & -1 & 0 & i & 0 \\ 0 & 0 & -i & -i & 0 & 0 \\ 1 & i & 0 & 0 & 0 & 0 \end{bmatrix} \begin{matrix} x\uparrow \\ y\uparrow \\ z\uparrow \\ x\downarrow \\ y\downarrow \\ z\downarrow \end{matrix}, \tag{23}$$

where Δ_0 is the zone center ($k=0$) spin-orbit splitting.

The valence-band structure of the unstrained semiconductor is obtained by calculating the eigenvalues of $H_{\mathbf{k}\cdot\mathbf{p}} + H_{\text{s.o.}}$, for appropriate values of L, M, N, and Δ_0. The values of L, M, N, and Δ_0 for Si and Ge are given in Table III. However, the values of these for the alloy, $Si_{1-x}Ge_x$, are obtained by linear interpolation: $L^{Si_{1-x}Ge_x} = (1-x)L^{Si} + xL^{Ge}$. The justification of this is as follows. Valence-band parameters A, B, and C, which are related to L, M, and N ($A = 1 + \frac{1}{3}(L+2M)$, $B = \frac{1}{3}(L-M)$, and $C^2 = \frac{1}{3}[N^2 - (L-M)^2]$), have been measured as a function of Ge content x.[24,25] While these parameters are found to vary with x for low-Si-content alloys, the experimental data are not sufficient to indicate the variation over a wide range of x. In the absence of experimental data, the simplest possible variation of these parameters with respect to x has been hypothesized, namely, a linear variation. This approach is supported by the experimental observation of a regular variation with x, without introducing unobserved features of a more complicated theory. The variation of Δ_0, on the other hand, has been rather completely measured over the full range of x,[26] and is well described by a linear interpola-

TABLE V. $Si_{1-x}Ge_x$ band-edge levels as a function of x. $E^{(000)}$, Ref. 5; $E^{(100)}$ and $E^{(111)}$, Ref. 8.

x	$E^{(000)}$ (eV)	x	$E^{(100)}$ (eV)	x	$E^{(111)}$ (eV)
0.0	4.0	0.0	1.110	0.0	1.65
0.543	2.245	0.033	1.08	0.85	0.86
0.653	1.914	0.043	1.072	0.87	0.838
0.774	1.503	0.0885	1.043	0.885	0.81
0.838	1.319	0.36	0.952	0.895	0.80
0.891	1.126	0.375	0.943	0.942	0.72
0.9355	1.042	0.445	0.92	0.975	0.67
1.0	0.8	0.598	0.893	1.0	0.645
		0.695	0.879		
		0.78	0.868		
		0.85	0.86		
		1.0	0.86		

tion between the values for Si and Ge.

The effects of strain on the electronic system of a semiconductor may be modeled using the deformation potential theory. The strain of interest in the present work is both static and uniform, arising from the epitaxy of a semiconductor film on a lattice-mismatched substrate. A deformation potential theory appropriate for dealing with this type of strain is covered in detail by Bir and Pikus.[27] Only the salient features of this will be outlined here.

Strain is incorporated into the band structure as a perturbative term in the calculation. The Hamiltonian of this perturbation, H_ε, has matrix elements of the form

$$H_{\varepsilon;ij}=\sum_{\alpha,\beta=1}^{3} D_{ij}^{\alpha\beta}\varepsilon_{\alpha\beta} , \tag{24}$$

where $\varepsilon_{\alpha\beta}$ is the (α,β) element of the strain tensor and $D_{ij}^{\alpha\beta}$ is a deformation potential. Since $D_{ij}^{\alpha\beta}$ bears the subscripts (i,j), it may be thought of as a matrix element of an operator $\underline{D}^{\alpha\beta}$, in the same way that $H_{\varepsilon;ij}$ is a matrix element of the operator $\underline{H}_\varepsilon$. Since there are nine strain tensor elements $\varepsilon_{\alpha\beta}$, there are correspondingly nine deformation potential operators $\underline{D}^{\alpha\beta}$. However, as $\varepsilon_{\alpha\beta}$ is symmetric, $\underline{D}^{\alpha\beta}$ is also symmetric with respect to α and β ($\underline{D}^{\alpha\beta}=\underline{D}^{\beta\alpha}$), leaving a maximum of only six independent operators. Also, it should be pointed out that as treated here, the effects of strain and spin-orbit coupling are independent. This means that it is sufficient to specify the form of $\underline{D}^{\alpha\beta}$ for spin-up states. As in the case of $\underline{H}_{\mathbf{k}\cdot\mathbf{p}}$, the operator will be block diagonal between spin-up and spin-down states, having the same form for both spins and no coupling terms between them.

At this point it is most efficient to consider the cases of specific interest to the present work: the deformation of a crystal of the cubic crystal class O_h. First, the nondegenerate levels of the conduction band are considered. Here the $\underline{D}^{\alpha\beta}$ are diagonal in (i,j) and may be treated as individual deformation potential constants. Symmetry under rotations about the [111] and [001] axes show that the Γ_2' level has only one independent deformation potential, D^{xx}, with the shift in energy of

$$\begin{aligned}\delta E^{(000)}&=\underline{H}_\varepsilon\\&=D^{xx}(\varepsilon_{xx}+\varepsilon_{yy}+\varepsilon_{zz}) .\end{aligned} \tag{25}$$

Conventionally, D^{xx} for this level is referred to as $\Xi_d^{(000)}$.

The Δ_1 conduction-band minima are the second energy levels of interest. These are characterized by constant energy surfaces which are ellipsoids of revolution whose major axes lie along their respective $\langle 100\rangle$ axes. Symmetry under rotation about [100] shows that the shift of a level along the [100] axis is

$$\delta E^{(100)}=D^{xx}\varepsilon_{xx}+D^{yy}(\varepsilon_{yy}+\varepsilon_{zz}) . \tag{26}$$

Conventionally, $D^{xx}=\Xi_d^{(100)}+\Xi_u^{(100)}$ and $D^{yy}=\Xi_d^{(100)}$. Accounting for the three distinct Δ_1 levels,

$$\begin{aligned}\delta E^{(100)}&=\Xi_d^{(100)}(\varepsilon_{xx}+\varepsilon_{yy}+\varepsilon_{zz})+\Xi_u^{(100)}\varepsilon_{xx} ,\\ \delta E^{(010)}&=\Xi_d^{(100)}(\varepsilon_{xx}+\varepsilon_{yy}+\varepsilon_{zz})+\Xi_u^{(100)}\varepsilon_{yy} ,\\ \delta E^{(001)}&=\Xi_d^{(100)}(\varepsilon_{xx}+\varepsilon_{yy}+\varepsilon_{zz})+\Xi_u^{(100)}\varepsilon_{zz} .\end{aligned} \tag{27}$$

The final conduction-band levels of interest are the L_1 minima. Rotations about the [111] axis show that there are only two independent deformation potentials:

$$\begin{aligned}D^{xx}&=\Xi_d^{(111)}+\tfrac{1}{3}\Xi_u^{(111)} ,\\ D^{xy}&=\tfrac{1}{3}\Xi_u^{(111)} .\end{aligned} \tag{28}$$

The energy shifts under strain are

$$\begin{aligned}\delta E^{(111)}&=(\Xi_d^{(111)}+\tfrac{1}{3}\Xi_u^{(111)})(\varepsilon_{xx}+\varepsilon_{yy}+\varepsilon_{zz})\\&\quad+\tfrac{2}{3}\Xi_u^{(111)}(\varepsilon_{xy}+\varepsilon_{yz}+\varepsilon_{zx}) ,\\ \delta E^{(11\bar1)}&=(\Xi_d^{(111)}+\tfrac{1}{3}\Xi_u^{(111)})(\varepsilon_{xx}+\varepsilon_{yy}+\varepsilon_{zz})\\&\quad+\tfrac{2}{3}\Xi_u^{(111)}(\varepsilon_{xy}-\varepsilon_{yz}-\varepsilon_{zx}) ,\\ \delta E^{(1\bar11)}&=(\Xi_d^{(111)}+\tfrac{1}{3}\Xi_u^{(111)})(\varepsilon_{xx}+\varepsilon_{yy}+\varepsilon_{zz})\\&\quad+\tfrac{2}{3}\Xi_u^{(111)}(-\varepsilon_{xy}-\varepsilon_{yz}+\varepsilon_{zx}) ,\\ \delta E^{(\bar111)}&=(\Xi_d^{(111)}+\tfrac{1}{3}\Xi_u^{(111)})(\varepsilon_{xx}+\varepsilon_{yy}+\varepsilon_{zz})\\&\quad+\tfrac{2}{3}\Xi_u^{(111)}(-\varepsilon_{xy}+\varepsilon_{yz}-\varepsilon_{zx}) .\end{aligned} \tag{29}$$

Numerical evaluation of the shifts in conduction-band levels requires a knowledge of the deformation potentials Ξ_d and Ξ_u. Reliable values for Ξ_u are available in the literature, and the values used in this work are given in Table II. However, Ξ_d, itself, is difficult to determine directly. More reliable data are available concerning the shift of the band gap with hydrostatic pressure. Defining a hydrostatic pressure deformation potential $\Xi_{\rm hyd}^{(\mathbf{k})}$:

$$\begin{aligned}\delta E_g(\mathbf{k})&=\delta E_c(\mathbf{k})-\delta E_v(\mathbf{0})\\&=\delta E_c(\mathbf{k})-a(\varepsilon_{xx}+\varepsilon_{yy}+\varepsilon_{zz})\\&=\Xi_{\rm hyd}^{(\mathbf{k})}(\varepsilon_{xx}+\varepsilon_{yy}+\varepsilon_{zz}) ,\end{aligned} \tag{30}$$

which is related to the pressure coefficient of the band gap:

$$\Xi_{\rm hyd}^{(\mathbf{k})}=-\tfrac{1}{3}(c_{11}+2c_{12})\frac{dE_g(\mathbf{k})}{dP} . \tag{31}$$

For $\langle 111\rangle$ valleys,

$$\Xi_{\rm hyd}^{(111)}=\Xi_d^{(111)}+\tfrac{1}{3}\Xi_u^{(111)}-a . \tag{32}$$

For $\langle 001\rangle$ valleys,

$$\Xi_{\rm hyd}^{(100)}=\Xi_d^{(100)}+\tfrac{1}{3}\Xi_u^{(100)}-a . \tag{33}$$

For the [000] valley,

$$\Xi_{\rm hyd}^{(000)}=\Xi_d^{(000)}-a . \tag{34}$$

In all cases, the parameter a is the valence band hydrostatic deformation potential. Values of $dE_g(\mathbf{k})/dP$ are given in Table II.

Partial symmetry is retained in the lattice of the strained film. Under a tetragonal distortion, arising from growth on a (001) substrate, the four L_1 conduction-band valleys ([111], [11$\bar1$], [1$\bar1$1], and [$\bar1$11]) are symmetrically equivalent and shift together under strain. Under the same distortion, the six Δ_1 valleys are not symmetrically equivalent, with the [100] and [010] valleys shifting to-

TABLE VI. Shifts and splittings of conduction-band levels in silicon under uniform biaxial strain $\varepsilon_{\parallel}=\pm 1\%$.

Substrate	Valley	$\varepsilon_{\parallel}=-0.01$	$\varepsilon_{\parallel}=0.00$	$\varepsilon_{\parallel}=+0.01$
(001)	[000]	4.015	4.000	3.985
	[100],[010]	1.039	1.110	1.181
	[001]	1.202	1.110	1.018
	$[111],[11\bar{1}],[1\bar{1}1],[\bar{1}11]$	1.710	1.650	1.590
(111)	[000]	4.020	4.000	3.980
	[100],[010],[001]	1.088	1.110	1.132
	[111]	1.879	1.650	1.421
	$[11\bar{1}],[1\bar{1}1],[\bar{1}11]$	1.675	1.650	1.625
(101)	[000]	4.019	4.000	3.981
	[100],[001]	1.113	1.110	1.107
	[010]	1.043	1.110	1.177
	$[111],[1\bar{1}1]$	1.803	1.650	1.497
	$[11\bar{1}],[\bar{1}11]$	1.643	1.650	1.657

gether and splitting from the [001] valley. The orientation of the substrate does affect the qualitative splitting of the valleys. Rhombohedral distortion, arising from growth on a (111) substrate, shifts the $[11\bar{1}]$, $[1\bar{1}1]$, and $[\bar{1}11]$ valleys together, splitting them from the [111] valley. Under this distortion, all Δ_1 valleys are symmetrically equivalent and shift together. Growth on a substrate of the third orientation considered in this work, (101), produces a monoclinic distortion and splits both the L_1 and Δ_1 levels. The [100] and [001] valleys are symmetrically equivalent, splitting from the [010] valley, while the [111] and $[1\bar{1}1]$ valleys are symmetrically equivalent and split from the $[11\bar{1}]$ and $[\bar{1}11]$ valleys, which themselves are symmetrically equivalent. A numerical example of this splitting is shown in Table VI, where the position of the conduction-band energy levels in Si under a lattice mismatch of $\varepsilon_{\parallel}=\pm 1\%$ is compared to their positions in unstrained material.

Of the conduction-band states considered in this work, the states which are degenerate in energy, neglecting twofold spin degeneracy (e.g., the $\langle 100\rangle$ valleys), have significantly differing wave vectors (e.g., $\mathbf{k}_{[100]}\neq\mathbf{k}_{[010]}$). Put another way, for any specific wave vector, no pair of conduction-band states, considered here, are degenerate or very close in energy. This means that any coupling between them is insignificant and therefore may be neglected. For large variations in wave vector (e.g., from an L_1 to a Δ_1 valley), the deformation potentials, used in this work, are taken to be different: $\Xi_u^{(111)}\neq\Xi_u^{(100)}$. However, for small variations in the wave vector (e.g., varying $\mathbf{k}$ in the vicinity of a Δ_1 valley), the deformation potentials are taken as constant, independent of the wave vector. To within the same degree of approximation, therefore, all conduction-band valleys shift rigidly under lattice deformation. That is, all points in the vicinity of a valley minimum shift by the same amount. Thus the shape of the valley is preserved, and the density-of-states effective mass is unaltered.

The valence-band deformation potential theory proves to be qualitatively different than that of the conduction band due to the threefold degeneracy of the Γ_{25}' representation. This leads to each operator $\underline{D}^{\alpha\beta}$ being expressible as a 3×3 matrix for each spin orientation. In the basis $|x\rangle,|y\rangle,|z\rangle$, used above, the operators $\underline{D}^{\alpha\beta}$ take the form

$$\underline{D}^{xx}=\begin{bmatrix} l & 0 & 0\\ 0 & m & 0\\ 0 & 0 & m\end{bmatrix},\quad \underline{D}^{yy}=\begin{bmatrix} m & 0 & 0\\ 0 & l & 0\\ 0 & 0 & m\end{bmatrix},$$

$$\underline{D}^{zz}=\begin{bmatrix} m & 0 & 0\\ 0 & m & 0\\ 0 & 0 & l\end{bmatrix},\quad \underline{D}^{xy}=\begin{bmatrix} 0 & \frac{n}{2} & 0\\ \frac{n}{2} & 0 & 0\\ 0 & 0 & 0\end{bmatrix}, \tag{35}$$

$$\underline{D}^{yz}=\begin{bmatrix} 0 & 0 & 0\\ 0 & 0 & \frac{n}{2}\\ 0 & \frac{n}{2} & 0\end{bmatrix},\quad \underline{D}^{zx}=\begin{bmatrix} 0 & 0 & \frac{n}{2}\\ 0 & 0 & 0\\ \frac{n}{2} & 0 & 0\end{bmatrix}\begin{matrix} x\\ y\\ z\end{matrix}.$$

These, whose form may be verified by considering the symmetry of the system, are due to Pikus and Bir.[28] Performing the sum [Eq. (24)] over α and β yields the matrix of the perturbation to the valence-band Hamiltonian, which is

$$\underline{H}_{\varepsilon}=\begin{bmatrix} \underline{H}'' & \underline{0}_{3\times 3}\\ \underline{0}_{3\times 3} & \underline{H}''\end{bmatrix}\begin{matrix}\uparrow\\ \downarrow\end{matrix}, \tag{36a}$$

$$\underline{H}''=\begin{bmatrix} l\varepsilon_{xx}+m(\varepsilon_{yy}+\varepsilon_{zz}) & n\varepsilon_{xy} & n\varepsilon_{zx}\\ n\varepsilon_{xy} & l\varepsilon_{yy}+m(\varepsilon_{zz}+\varepsilon_{xx}) & n\varepsilon_{yz}\\ n\varepsilon_{zx} & n\varepsilon_{yz} & l\varepsilon_{zz}+m(\varepsilon_{xx}+\varepsilon_{yy})\end{bmatrix}\begin{matrix} x\\ y\\ z\end{matrix}. \tag{36b}$$

The quantities l, m, and n are three independent valence-band deformation potentials and are related to the more commonly appearing potentials a, b, and d:

$$a=\frac{l+2m}{3}\ ,$$
$$b=\frac{l-m}{3}\ , \tag{37}$$
$$d=\frac{n}{\sqrt{3}}\ .$$

In contrast to the conduction band (again, neglecting spin degeneracy), the states of the valence band, whose wave vectors lie near the center of the Brillouin zone, will be either degenerate or very close to one another in energy, and so are significantly coupled to one another. Again, the involved deformation potentials themselves are independent of wave vector for points in the vicinity of the center of the Brillouin zone. However, the significant coupling between the valence-band states leads to a strong mixing of those states under strain perturbation. Also, the $\mathbf{k}\cdot\mathbf{p}$ interaction between these states results in a change in the shape of the band structure when under strain perturbation. This, of course, means that the density-of-states effective mass in the valence band can vary significantly as the lattice is distorted.

In order to discuss the nature of the valence band under strain perturbation, it will be convenient to first transform to another basis for the eigenstates. The transformation is from the original basis of $|i\alpha\rangle$, $i=x,y,z$, $\alpha=\uparrow,\downarrow$, to the basis whose elements have the rotational symmetry of the eigenfunctions of the total angular momentum operator squared and its z component: $\mathbf{J}\cdot\mathbf{J}$ and J_z, respectively. The new basis states are the familiar $|j,m_j\rangle$ states with $j=\frac{3}{2}$, $m_j=\pm\frac{3}{2},\pm\frac{1}{2}$, and $j=\frac{1}{2}$, $m_j=\pm\frac{1}{2}$. The matrix of the transformation to the new basis is the same as that which diagonalizes the spin-orbit perturbation Hamiltonian $\underline{A}\,\underline{H}_{\text{s.o.}}\,\underline{A}^{\dagger}$ and is

$$\underline{A}=\begin{array}{c}\begin{matrix} i,\alpha: & x\uparrow & y\uparrow & z\uparrow & x\downarrow & y\downarrow & z\downarrow & j,m_j \end{matrix}\\ \left[\begin{array}{cccccc} -1/\sqrt{2} & i/\sqrt{2} & 0 & 0 & 0 & 0 & \frac{3}{2},\frac{3}{2} \\ 1/\sqrt{6} & i/\sqrt{6} & 0 & 0 & 0 & \sqrt{2/3} & \frac{3}{2},-\frac{1}{2} \\ -1/\sqrt{3} & -i/\sqrt{3} & 0 & 0 & 0 & 1/\sqrt{3} & \frac{1}{2},-\frac{1}{2} \\ 0 & 0 & 0 & 1/\sqrt{2} & i/\sqrt{2} & 0 & \frac{3}{2},-\frac{3}{2} \\ 0 & 0 & \sqrt{2/3} & -1/\sqrt{6} & i/\sqrt{6} & 0 & \frac{3}{2},\frac{1}{2} \\ 0 & 0 & -1/\sqrt{3} & -1/\sqrt{3} & i/\sqrt{3} & 0 & \frac{1}{2},\frac{1}{2} \end{array}\right] \end{array}\ . \tag{38}$$

Adoption of the new basis will make the description of the valence-band eigenstates clearer.

Simple examples of the effect of strain on the valence band are now considered. Additional complications associated with varying the material parameters to describe the effect of alloying are avoided at this point by considering a Si film which is subjected to varying degrees of strain, which might, for example, be achievable by using different substrates. Each of the three substrate orientations (001), (111), and (101) will be examined in turn.

First, the (001) substrate is considered. Figure 1(a) shows the shifts of the valence-band levels at $k=0$, in Si, relative to the valence-band edge (at energy E_1), for biaxial strain $\varepsilon_{\parallel}$ ranging from -0.02 to $+0.02$. The three energies are labeled E_1, E_2, and E_3 in order of decreasing energy. For biaxial compressive strain ($\varepsilon_{\parallel}<0$), the separation of E_1 and E_2 is seen to be quite nonlinear. This nonlinearity becomes apparent for shifts which are on the order of the spin-orbit splitting Δ_0. If a material with a larger spin-orbit splitting, such as Ge ($\Delta_0=0.282$ eV), is subjected to the same degree of biaxial compressive strain, the shift of E_2 relative to E_1 is on the same order as that in Si and is rather linear in $\varepsilon_{\parallel}$, being much less than Δ_0. For the (001) substrate, the splittings E_1-E_2 and E_1-E_3 may be analytically determined, and are, for $\varepsilon_{\parallel}<0$,

$$E_1-E_2=\tfrac{1}{2}(\Delta_0-h)-\tfrac{1}{6}[(h+3\Delta_0)^2+8h^2]^{1/2}\ , \tag{39}$$
$$E_1-E_3=\tfrac{1}{2}(\Delta_0-h)+\tfrac{1}{6}[(h+3\Delta_0)^2+8h^2]^{1/2}\ , \tag{40}$$

and, for $\varepsilon_{\parallel}>0$,

$$E_1-E_2=-\tfrac{1}{2}(\Delta_0-h)+\tfrac{1}{6}[(h+3\Delta_0)^2+8h^2]^{1/2}\ , \tag{41}$$
$$E_1-E_3=\tfrac{1}{3}[(h+3\Delta_0)^2+8h^2]^{1/2}\ , \tag{42}$$
$$h=-3b(1+1/\sigma^{(001)})\varepsilon_{\parallel}\ , \tag{43}$$

where b is one of the deformation potentials presented above [Eq. (37)]. The first of these equations clarifies the asymptotic behavior discussed above. As compressive strain is increased, E_1-E_2 approaches the asymptotic limit of $2\Delta_0/3$. For all biaxial compressive strain which is of such a magnitude that it can be validly treated as a perturbation, the Brillouin-zone splitting between light and heavy hole will not exceed $2\Delta_0/3$ [for (001) substrates].

Corresponding to the eigenvalues plotted in Fig. 1(a), are the valence-band eigenvectors, whose squared com-

ponents are plotted in Figs. 1(b)–1(d). The strain perturbation mixes the $|\frac{3}{2},-\frac{1}{2}\rangle$ state with the $|\frac{1}{2},-\frac{1}{2}\rangle$ state and the $|\frac{3}{2},\frac{1}{2}\rangle$ state with the $|\frac{1}{2},\frac{1}{2}\rangle$ state at $\mathbf{k}=0$. For this substrate orientation, no other strain-induced mixing occurs. The mixing of states is clarified by considering a 90° rotation of each basis state about the substrate normal. The effect on $|j,m_j\rangle$ of a rotation through an angle φ about the axis of angular momentum quantization is to multiply the state by an overall phase factor of $e^{im_j\varphi}$. Eigenstates of the strain-perturbed system must retain the same relative phase between their constituent basis states under all symmetry operations. One such symmetry operation is a 90° rotation about the substrate normal. Only basis states with the same value of m_j receive the same phase factor, and thus only states with the same value of m_j may be mixed by the perturbation. The valence-band edge, under compressive biaxial strain ($\varepsilon_\parallel<0$), is characterized by the $|\frac{3}{2},\pm\frac{3}{2}\rangle$ states. Under biaxial tensile strain, the band edge is characterized by a strain-dependent mixture of $|\frac{3}{2},\pm\frac{1}{2}\rangle$ and $|\frac{1}{2},\pm\frac{1}{2}\rangle$ states, being dominantly $|\frac{3}{2},\pm\frac{1}{2}\rangle$ for low values of strain. This difference between compressive and tensile strain is the well-known interchange of heavy and light hole between the two strain cases. The lowest energy eigenvalue always corresponds to a strain-dependent mixture of $|\frac{3}{2},\pm\frac{1}{2}\rangle$ and $|\frac{1}{2},\pm\frac{1}{2}\rangle$ states, which is dominantly $|\frac{1}{2},\pm\frac{1}{2}\rangle$ for low values of strain.

Before discussing the other two substrate orientations, another basis transformation should be introduced. As may be expected, biaxial strain arising from a (111) or a (101) substrate, which, respectively, appears as a rhombohedral or a monoclinic distortion to the lattice, will mix the states $|j,m_j\rangle$ in a nonsimple way. However, when the distorted lattice is viewed from a coordinate system whose z axis is normal to the substrate, the distortions are qualitatively the same as the tetragonal distortion of the (001) substrate. The required coordinate system is the (x',y',z') system, introduced in Sec. II. As discussed in Sec. II, in this coordinate system no shear is present, $\varepsilon'_{12}=\varepsilon'_{23}=\varepsilon'_{31}=0$, and the distortion is $\varepsilon'_{11}=\varepsilon'_{22}=\varepsilon_\parallel$, $\varepsilon'_{33}=-\varepsilon_\parallel/\sigma$. Now, if the basis states $|j,m_j\rangle$ are rotated so as to make the axis of angular

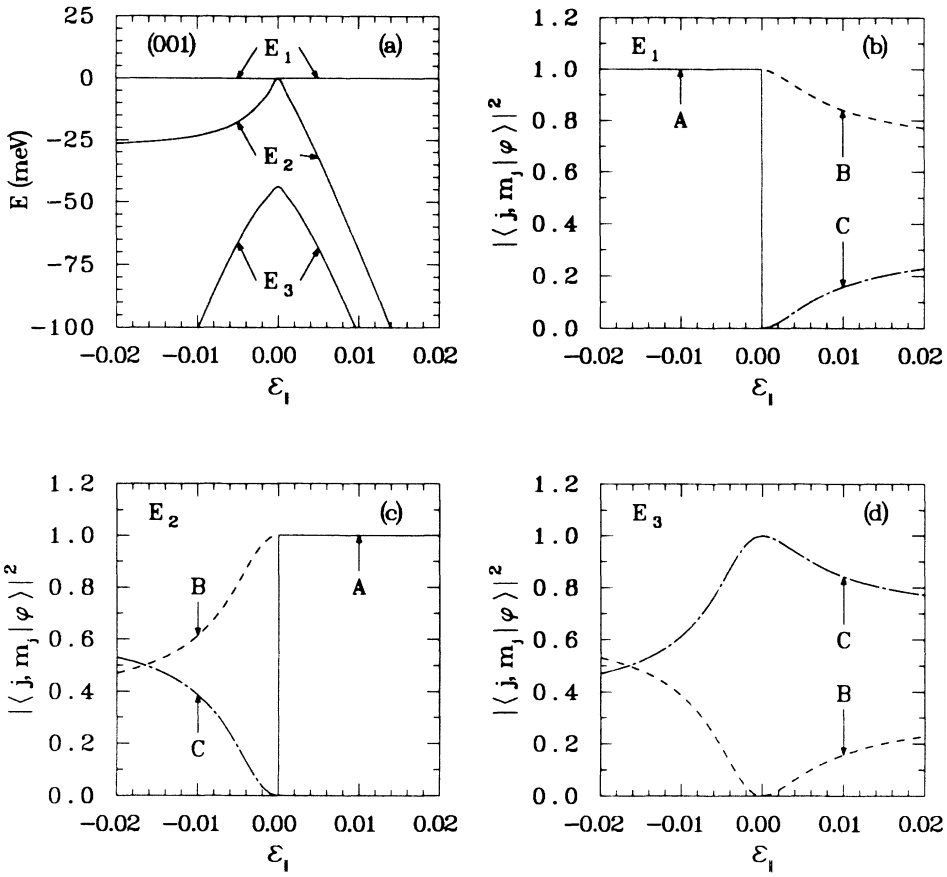

FIG. 1. Valence band at $k=0$ in Si film on (001) substrate. (a) Shifts of the valence-band-energy levels as a function of biaxial strain $\varepsilon_\parallel$. $\varepsilon_\parallel<0$, biaxial compressive strain; $\varepsilon_\parallel>0$, biaxial tensile strain. E_1, valence-band edge; E_1,E_2,E_3, energy eigenvalues in order of decreasing energy. (b) Squared eigenvector (φ) components corresponding to eigenvalue E_1. $A=|\langle\frac{3}{2},\pm\frac{3}{2}|\varphi\rangle|^2$, $B=|\langle\frac{3}{2},\pm\frac{1}{2}|\varphi\rangle|^2$ and $C=|\langle\frac{1}{2},\pm\frac{1}{2}|\varphi\rangle|^2$. (c) Squared eigenvector (φ) components corresponding to eigenvalue E_2. A, B, and C defined as in (b). (d) Squared eigenvector (φ) components corresponding to eigenvalue E_3. A, B, and C defined as in (b). $A=0$ for all values of $\varepsilon_\parallel$.

momentum quantization be the z' axis, then mixing between the new states should be simpler, as in the case of the (001) substrate. The transformation of the basis states may be represented by the matrix $\underline{N}$, whose action is, schematically,

$$|j',m_j'\rangle = \underline{N}|j,m_j\rangle \ . \tag{44}$$

The matrix $\underline{N}$ may be determined using the elementary mathematics of spinor rotation and is found to be[29]

$$\underline{N}= \begin{array}{c} \begin{matrix} j,m_j: & \frac{3}{2},\frac{3}{2} & \frac{3}{2},-\frac{1}{2} & \frac{1}{2},-\frac{1}{2} & \frac{3}{2},-\frac{3}{2} & \frac{3}{2},\frac{1}{2} & \frac{1}{2},\frac{1}{2} & j',m_j' \end{matrix} \\ \begin{bmatrix} a^3 & \sqrt{3}ac^2 & 0 & c^3 & \sqrt{3}a^2c & 0 & \frac{3}{2},\frac{3}{2} \\ \sqrt{3}ab^2 & 2bcd+ad^2 & 0 & \sqrt{3}cd^2 & 2abd+b^2c & 0 & \frac{3}{2},-\frac{1}{2} \\ 0 & 0 & d & 0 & 0 & b & \frac{1}{2},-\frac{1}{2} \\ b^3 & \sqrt{3}bd^2 & 0 & a^3 & \sqrt{3}b^2d & 0 & \frac{3}{2},-\frac{3}{2} \\ \sqrt{3}a^2b & 2acd+bc^2 & 0 & \sqrt{3}c^2d & 2abc+a^2d & 0 & \frac{3}{2},\frac{1}{2} \\ 0 & 0 & c & 0 & 0 & a & \frac{1}{2},\frac{1}{2} \end{bmatrix} \end{array} , \tag{45}$$

with

$$\begin{aligned} a &= \cos(\theta/2) \ , \\ b &= -e^{i\varphi}\sin(\theta/2) \ , \\ c &= e^{-i\varphi}\sin(\theta/2) \ , \\ d &= \cos(\theta/2) \ , \end{aligned} \tag{46}$$

where θ and φ orient the substrate normal z' relative to (x,y,z), as in Sec. II.

Now the (111) substrate can be considered. Figure 2(a) shows the shifts of the valence-band levels in Si, relative to the valence-band edge, for biaxial strain $\varepsilon_{\parallel}$, ranging from -0.02 to $+0.02$. Again, the three energies are labeled E_1, E_2, and E_3 in order of decreasing energy. The shift of the bands is nearly identical to those in the case of the (001) substrate. This similarity is not fundamental, but rather is a fortuitous result of the specific numerical values of the deformation potentials b and d in Si. Here, as well, the splittings E_1-E_2 and E_1-E_3 may be analytically determined. They are, for $\varepsilon_{\parallel}<0$,

$$E_1-E_2=\tfrac{1}{2}(\Delta_0-3h)-\tfrac{1}{2}[(h+\Delta_0)^2+8h^2]^{1/2} \ , \tag{47}$$

$$E_1-E_3=\tfrac{1}{2}(\Delta_0-3h)+\tfrac{1}{2}[(h+\Delta_0)^2+8h^2]^{1/2} \ , \tag{48}$$

and, for $\varepsilon_{\parallel}>0$,

$$E_1-E_2=-\tfrac{1}{2}(\Delta_0-3h)+\tfrac{1}{2}[(h+\Delta_0)^2+8h^2]^{1/2} \ , \tag{49}$$

$$E_1-E_3=[(h+\Delta_0)^2+8h^2]^{1/2} \ , \tag{50}$$

$$h=-\frac{1}{\sqrt{3}}d(1+1/\sigma^{(111)})\varepsilon_{\parallel} \ , \tag{51}$$

where d is one of the valence-band deformation potentials. The first of these equations again clarifies the asymptotic behavior of E_1-E_2 for $\varepsilon_{\parallel}<0$ shown in Fig. 2(a). Here, as in the case of the (001) substrate, E_1-E_2 approaches the same asymptotic limit of $2\Delta_0/3$ as biaxial compressive strain is increased. Of course, the same qualification applies, namely, that the strain be small enough to be validly treated as a perturbation.

Figures 2(b)–2(d) show the squared components of the eigenvectors for the valence-band states corresponding to the eigenvalues of Fig. 2(a). The components are relative to a basis which has been rotated by the transformation N [Eq. (45)]. The appropriate angles of substrate orientation to evaluate a, b, c, and d [Eq. (46)] are $\theta=\arccos(1/\sqrt{3})$ and $\varphi=\pi/4$. The angular momentum is quantized along the [111] axis with quantum number m_j. The strain-induced mixing of basis states for the (111) substrate, shown in Figs. 2(b)–2(d), is virtually identical to the mixing for the (001) substrate. Here, again, this similarity is not fundamental, as mentioned before. The [111] axis is an axis of threefold rotational symmetry for the strained epitaxial film. Following the argument presented above for the (001) substrate, it can be seen that eigenstate invariance under $\pm 120°$ rotations about [111] permits mixing only of basis states with the same value of m_j. Thus, again, the strain perturbation mixes the $|\frac{3}{2},-\frac{1}{2}\rangle$ state with the $|\frac{1}{2},-\frac{1}{2}\rangle$ state and the $|\frac{3}{2},\frac{1}{2}\rangle$ state with the $|\frac{1}{2},\frac{1}{2}\rangle$ state at $\mathbf{k}=\mathbf{0}$. For this substrate orientation, like the (001) substrate, no other strain-induced mixing occurs.

The nature of the valence band of a strained film on a (101) substrate is somewhat more complicated than for films on (001) and (111) substrates. Figure 3(a) shows the shifts of the valence-band levels in Si, relative to the valence-band edge, for biaxial strain $\varepsilon_{\parallel}$, ranging from -0.02 to $+0.02$. The shift in the bands is obviously

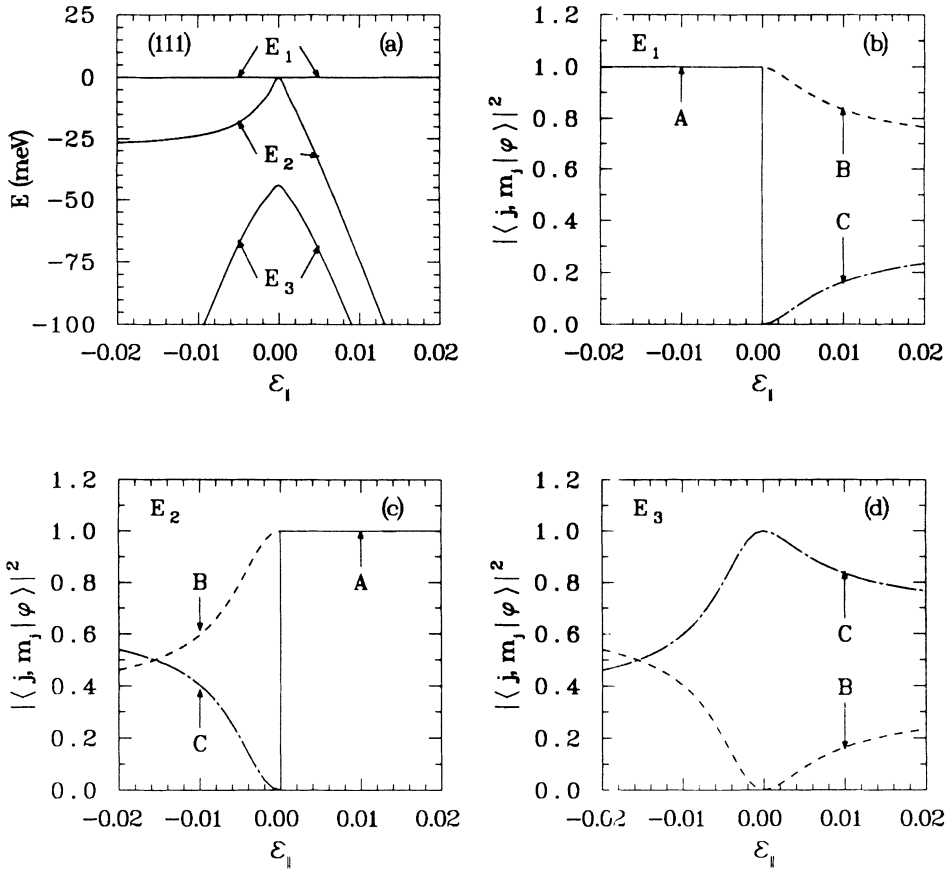

FIG. 2. Valence band at $k=0$ in Si film on (111) substrate. (a) Shifts of the valence-band-energy levels as a function of biaxial strain $\varepsilon_{\parallel}$. $\varepsilon_{\parallel}<0$, biaxial compressive strain; $\varepsilon_{\parallel}>0$, biaxial tensile strain. E_1, valence-band edge; E_1,E_2,E_3, energy eigenvalues in order of decreasing energy. (b) Squared eigenvector (φ) components corresponding to eigenvalue E_1. $A=|\langle \frac{3}{2},\pm\frac{3}{2}|\varphi\rangle|^2$, $B=|\langle \frac{3}{2},\pm\frac{1}{2}|\varphi\rangle|^2$, and $C=|\langle \frac{1}{2},\pm\frac{1}{2}|\varphi\rangle|^2$. (c) Squared eigenvector (φ) components corresponding to eigenvalue E_2. A, B, and C defined as in (b). (d) Squared eigenvector (φ) components corresponding to eigenvalue E_3. A, B, and C defined as in (b). $A=0$ for all values of $\varepsilon_{\parallel}$.

different than in the cases of (001) and (111) substrates. This is particularly apparent for the heavy-hole–light-hole splitting, E_1-E_2, for compressive strain, $\varepsilon_{\parallel}<0$. Unfortunately, because of more extensive mixing of the basis states, to be discussed below, the analytic expressions for the splittings E_1-E_2 and E_1-E_3 are very complicated, unlike Eqs. (39)–(42) and (47)–(50). Because of their complexity, their use is impractical, and therefore they are not reported here.

Figures 3(b)–3(d) show the components of the eigenvectors corresponding to the eigenvalues of Fig. 3(a). The basis has been rotated, with $\theta=\pi/4$, $\varphi=0$. The angular momentum is quantized along the [101] axis. The [101] axis is a twofold axis of rotational symmetry for the epitaxial film. Under a 180° rotation about the [101] axis, the basis states acquire a phase factor of $e^{im_j\pi}$. Considering $m_j=+\frac{3}{2}$ and $-\frac{1}{2}$ states, it is found that these may now mix under strain perturbation, since $e^{i3\pi/2}=e^{-i\pi/2}$. In other words, $|\frac{3}{2},\frac{3}{2}\rangle,|\frac{3}{2},-\frac{1}{2}\rangle,|\frac{1}{2}-\frac{1}{2}\rangle$ all receive the same phase factor under a rotation of 180° about [101]. Thus an eigenstate may be a linear combination of these three basis states. Of course $m_j=-\frac{3}{2}$ and $+\frac{1}{2}$ states may mix with each other, as well. This is the basis of the complexity of the analytic expressions for E_1-E_2 and E_1-E_3. In both of the cases of the (001) and (111) substrates, because the $m_j=\pm\frac{3}{2}$ states did not mix with the $m_j=\pm\frac{1}{2}$ states, the Hamiltonian matrix had the block diagonal form of 1×1 ($m_j=\pm\frac{3}{2}$) and 2×2 ($m_j=\pm\frac{1}{2}$) submatrices. The secular equation is written as products of first-order (1×1 blocks) and second-order (2×2 blocks) polynomials. The solutions for E_1, E_2, and E_3 of such are quite simple. However, in the present case of the (101) substrate, the Hamiltonian matrix has the block diagonal form of two 3×3 submatrices ($m_j=\pm\frac{3}{2},\mp\frac{1}{2}$ mixing terms in each). The secular equation has the form of the square of a third-order polynomial. Although analytic solutions to third-order polynomials are theoretically possible, they are generally quite complicated. Unfortunately, this is true in the present case.

The degree of this mixing is shown in Figs. 3(b)–3(d). For low degrees of biaxial strain, the valence-band edge is dominantly $|\frac{3}{2},\pm\frac{3}{2}\rangle$-like or $|\frac{3}{2},\pm\frac{1}{2}\rangle$-like, for compressive

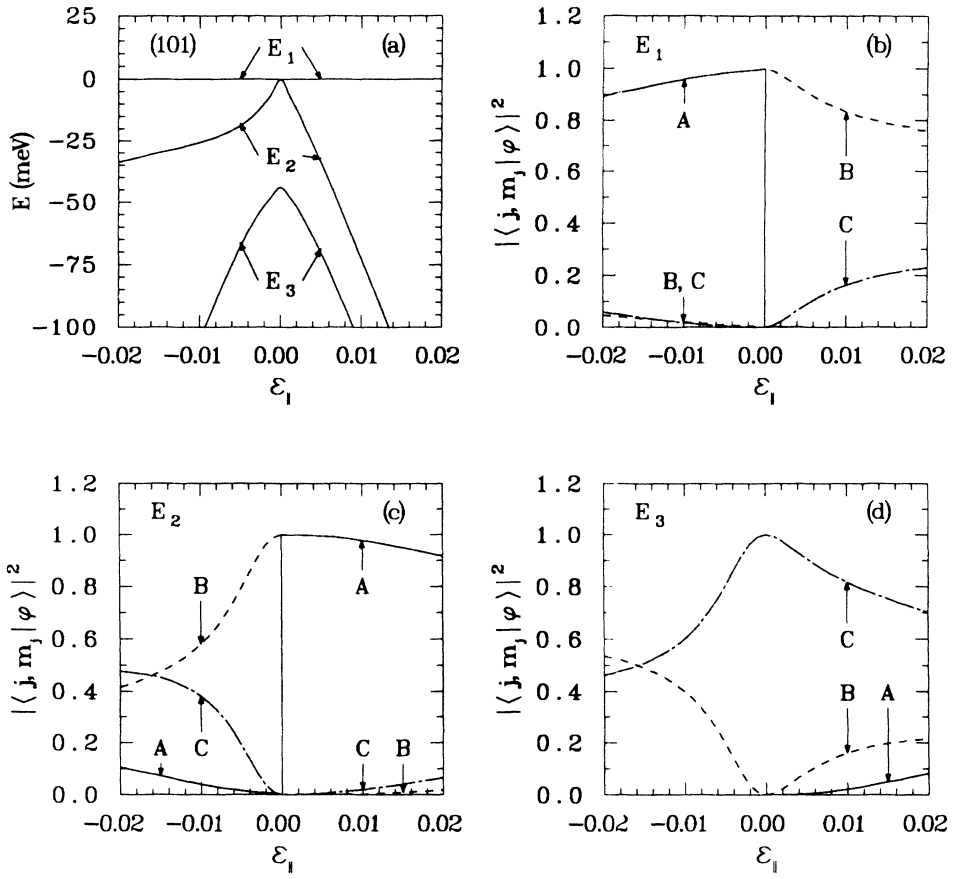

FIG. 3. Valence band at $k=0$ in Si film on (101) substrate. (a) Shifts of the valence-band-energy levels as a function of biaxial strain $\varepsilon_{\parallel}$. $\varepsilon_{\parallel}<0$, biaxial compressive strain; $\varepsilon_{\parallel}>0$, biaxial tensile strain. E_1, valence-band edge; E_1, E_2, E_3, energy eigenvalues in order of decreasing energy. (b) Squared eigenvector (φ) components corresponding to eigenvalue E_1. $A=|\langle \frac{3}{2},\pm\frac{3}{2}|\varphi\rangle|^2$, $B=|\langle \frac{3}{2},\pm\frac{1}{2}|\varphi\rangle|^2$, and $C=|\langle \frac{1}{2},\pm\frac{1}{2}|\varphi\rangle|^2$. (c) Squared eigenvector (φ) components corresponding to eigenvalue E_2. A, B, and C defined as in (b). (d) Squared eigenvector (φ) components corresponding to eigenvalue E_3. A, B, and C defined as in (b).

or tensile strain, respectively. The most notable distinction from earlier cases is that as the compressive strain is increased, the band-edge state does not remain purely $|\frac{3}{2},\pm\frac{3}{2}\rangle$, but mixes in an appreciable amount of $|\frac{3}{2},\pm\frac{1}{2}\rangle$ and $|\frac{1}{2},\pm\frac{1}{2}\rangle$. Similar anomalous mixing is seen to occur for the second eigenstate (eigenvalue E_2) under both compressive and tensile strain, and for the third eigenstate (eigenvalue E_3) under tensile strain.

In conclusion of this section, it should be noted that in passing from higher to lower symmetry substrates, more mixing of basis states is permitted. For the most general substrate, such as discussed in the Appendix, the normal is not an axis of rotational symmetry (more precisely, it is an axis of onefold rotational symmetry). Since the only rotational symmetry operation for a film on such a substrate is a 360° rotation about the normal, all six basis states may mix under strain perturbation. Each basis state, under such a rotation, receives a phase factor of -1.

IV. INTRINSIC PROPERTIES

Having outlined the method used to determine both the valence- and conduction-band structure, the method of calculating the intrinsic Fermi energy and carrier concentration as well as the band-edge effective densities of states are briefly presented here. Since the complicated effects of strain on impurity levels, especially shallow acceptor levels, is not within the scope of this work, the following discussion is confined to the determination of the intrinsic carrier concentration n_i. The physical requirement of charge neutrality is clearly met: $n_i=n=p$. This condition is the basis for the simultaneous determination of the Fermi energy and the intrinsic carrier concentration. These come from the solution to the equation

$$n=p\ ,$$
$$n=\int_0^{\infty} D_c(E)\frac{1}{1+e^{(E+E_g-E_i)/kT}}dE\ , \tag{52}$$
$$p=\int_{-\infty}^{0} D_v(-E)\frac{1}{1+e^{(E_i-E)/kT}}dE\ .$$

The parameters above are E, energy; E_g, band gap; E_i, Fermi energy; kT, product of Boltzmann's constant and temperature; D_c, conduction-band density of states; D_v, valence-band density of states; n, free-electron concentration; and p, free-hole concentration.

The conduction-band density of states is derived in the standard way, assuming parabolic dispersion and ellipsoidal (L_1, Δ_1) or spherical (Γ_2') constant energy surfaces. For a given valley at energy E_0, the formula is

$$D_c = \begin{cases} \sqrt{2}\dfrac{(m_d^*)^{3/2}\sqrt{E-E_0}}{\pi^2\hbar^3}, & E \geq E_0 \\ 0, & E < E_0 \end{cases} . \tag{53}$$

The total conduction-band density of states is the sum of such terms over all conduction-band valleys. The density-of-states effective masses m_d^* for Ge (Γ_2' and L_1) and Si (Δ_1) are given in Table II. These masses are presumed to not change significantly with alloying and strain, as discussed in Sec. III.

The valence-band density of states D_v is obtained by numerical integration over the three valence-band constant energy surfaces (heavy, light, and split-off hole). The formula used is

$$D_v = \frac{2}{(2\pi)^3}\int \frac{k^2}{|\nabla_k E|} d\Omega . \tag{54}$$

In this formula, k is the magnitude of the wave vector lying on the constant energy surface at polar coordinates θ, φ. The gradient of energy with respect to wave vector is evaluated on the constant energy surface. The differential solid angle has the standard meaning: $d\Omega = \sin\theta\, d\theta\, d\varphi$. The numerical approach is necessary because the three valence bands are strongly coupled. Strain perturbation in shifting the relative positions of the valence bands will affect the degree of their coupling and thereby change their shape and density of states, as discussed in Sec. III.

Having simultaneously determined n_i and E_i from Eqs. (52), the band-edge effective densities of state are very simply determined from

$$\begin{aligned} N_c &= n_i e^{(E_g - E_i)/kT} \quad \text{(conduction band)} , \\ N_v &= n_i e^{E_i/kT} \quad \text{(valence band)} . \end{aligned} \tag{55}$$

Table VII shows values of E_i, n_i, N_c, and N_v in Si as a function of biaxial strain for Si films grown on (001), (111), and (101) substrates. Strain is seen to generally have a stronger effect on N_v than on N_c, due to its greater effect on valence-band curvature than on conduction-band curvature. Variation of N_c with strain is primarily due to the strain-induced separation and crossing of valleys, changing the number and identity (Δ_1 or L_1) valleys at the band edge.

V. PSEUDOMORPHIC $Si_{1-x}Ge_x$ FILMS

The effects of substrate composition and crystallographic orientation on the alloy band structure and intrinsic properties are presented graphically in this section in Figs. 4–12. Three substrate compositions are considered: Si, Ge, and $Si_{0.5}Ge_{0.5}$. The epitaxial alloy film is under biaxial compressive strain ($\varepsilon_\parallel < 0$) when grown on a Si substrate. Growth on a Ge substrate results in biaxial tensile strain ($\varepsilon_\parallel > 0$). Growth of $Si_{1-x}Ge_x$ on $Si_{0.5}Ge_{0.5}$ will result in either compressive ($x > 0.5$) or tensile ($x < 0.5$) strain in the epitaxial film. For each substrate composition, three orientations are considered: (001), (111), and (101). The methods used to calculate the data presented in this section are as outlined in Secs. II–IV.

The configuration shown in Fig. 4 is the most common: $Si_{1-x}Ge_x$/Si(001). As x increases, the film is under increasing biaxial compressive strain. Figure 4(a) shows that both the band gap (C–E) and intrinsic Fermi energy (D) decrease. The strained-layer conduction-band edge (C) is characterized by the two Δ_1 valleys [100] and [010]. The valence-band edge (E) is characterized by the heavy-hole state $|\frac{3}{2}, \pm\frac{3}{2}\rangle$. The [001] conduction-band valley (B), whose wave vector lies perpendicular to the substrate, splits from the other Δ_1 valleys and shifts to higher energy. All L_1 conduction-band valleys (A), being symmetrically equivalent under this lattice distortion, increase in energy above their bulk value. The light- (F) and heavy- (E) hole valence-band-edge degeneracy is lifted, and the split-off hole energy (G) shifts below its bulk value. Figure 4(b) shows a decrease, with increasing x, in both the conduction- and valence-band-edge effective densities of state N_c and N_v. The decrease in N_c is directly related to the splitting of the Δ_1 conduction-band valleys. As the [001] valley rises above the [100] and [010] valleys, the value of N_c decreases in proportion, from approximately 3×10^{19} to 2×10^{19} cm^{-3}. The decrease in N_v is the compound effect of two factors. The first factor is the splitting of the light- and heavy-hole levels. The second factor is the decrease in the valence-band density of states with strain and alloying. Despite the decrease in

TABLE VII. Calculated intrinsic Fermi energy E_i, intrinsic carrier concentrations n_i, and band-edge effective densities of state N_c and N_v in Si as dependent on strain and substrate orientation.

Substrate	$\varepsilon_\parallel$	E_i (eV)	n_i (cm^{-3})	N_v (cm^{-3})	N_c (cm^{-3})
bulk	0.00	0.552	1.38×10^{10}	2.64×10^{19}	3.21×10^{19}
(001)	−0.01	0.515	3.36×10^{10}	1.49×10^{19}	2.14×10^{19}
	+0.01	0.507	2.75×10^{10}	8.97×10^{18}	1.07×10^{19}
(111)	−0.01	0.536	1.66×10^{10}	1.65×10^{19}	3.21×10^{19}
	+0.01	0.552	5.81×10^{9}	1.07×10^{19}	3.21×10^{19}
(101)	−0.01	0.525	2.37×10^{10}	1.54×10^{19}	1.22×10^{19}
	+0.01	0.544	7.66×10^{9}	1.07×10^{19}	2.21×10^{19}

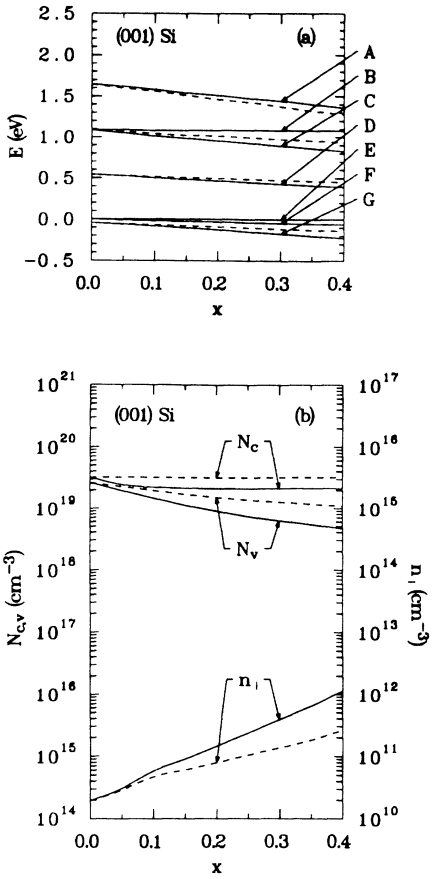

FIG. 4. $Si_{1-x}Ge_x/Si(001)$. (a) Band-structure shifts as a function of Ge mole fraction x. Solid lines, energy levels in strained alloy film; dashed lines, energy levels in bulk alloy. A, [111], [11$\bar{1}$], [1$\bar{1}$1], and [$\bar{1}$11] valleys, conduction band; B, [001] valley, conduction band; C, [100] and [010] valleys, conduction band; D, Fermi energy; E, valence-band edge (E_1); F, valence-band level E_2; G, valence-band level E_3. (b) Band-edge effective densities of state, N_c and N_v, and intrinsic carrier concentration n_i, as a function of Ge mole fraction x. Solid lines, values in strained alloy film; dashed lines, values in bulk alloy.

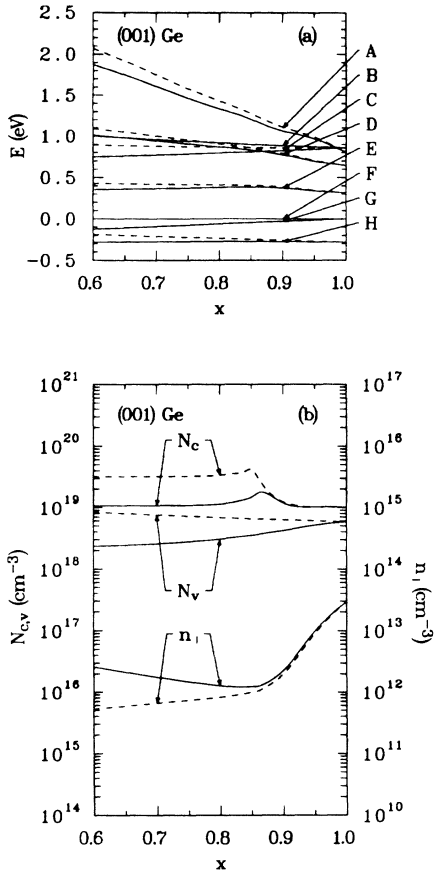

FIG. 5. $Si_{1-x}Ge_x/Ge(001)$. (a) Band-structure shifts as a function of Ge mole fraction x. Solid lines, energy levels in strained alloy film; dashed lines, energy levels in bulk alloy. A, [000] valley, conduction band; B, [100] and [010] valleys, conduction band; C, [001] valley, conduction band; D, [111], [11$\bar{1}$], [1$\bar{1}$1], and [$\bar{1}$11] valleys, conduction band; E, Fermi energy; F, valence-band edge (E_1); G, valence-band level E_2; H, valence-band level E_3. (b) Band-edge effective densities of state, N_c and N_v, and intrinsic carrier concentration n_i, as a function of Ge mole fraction x. Solid lines, values in strained alloy film; dashed lines, values in bulk alloy.

N_c and N_v, the intrinsic carrier concentration n_i increases above its bulk value with x. This is due to the decrease in band gap, upon which n_i depends exponentially.

The data for the Ge(001) substrate are shown in Fig. 5. In contrast to the previous case, the film is under biaxial tensile strain. This reverses the direction of the conduction-band valley shifts. Also, for high-Ge-content alloys, the Γ_2' valley (A) is near the conduction-band edge. The well-known[8] Δ_1-L_1 conduction-band-edge crossover shifts with strain, from 85% Ge to 87% Ge, where the band gap is maximum. At lower Ge concentrations ($x<0.87$) the conduction-band edge is characterized by the [001] valley (C). For $x>0.87$, the conduction-band edge is characterized by the four L_1 valleys (D). Over the entire composition range, the valence-band edge is characterized by the light-hole state which is a combination of $|\frac{3}{2},\pm\frac{1}{2}\rangle$ and $|\frac{1}{2},\pm\frac{1}{2}\rangle$ states. The [100] and [010] valleys (B) split from the [001] valley and rise to higher energy. The light- and heavy-hole degeneracy is lifted at the valence-band edge, with the heavy hole (G), $|\frac{3}{2},\pm\frac{3}{2}\rangle$, descending below the light hole. The split-off hole energy (H) shifts below its bulk value with increasing strain. Although shown in Fig. 5(a), the Γ_2' valley is insignificant in determining N_c, N_v, and n_i because of its very low effective mass compared to the other conduction-band valleys. The value of N_c, shown in Fig. 5(b), exhibits a peak, both for the bulk and strained cases. This arises from the Δ_1-L_1 conduction-band-edge crossover, at which point the number of valleys at the conduction-band edge is significantly increased. At Ge concentrations somewhat above crossover, N_c returns to nearly its bulk value. This is because the conduction-band edge, consisting of four L_1 valleys, is nearly identical between the two cases of strained and bulk material. At Ge concentrations somewhat below crossover, N_c drops below its bulk value from approximately 3×10^{19} to 1×10^{19} cm^{-2}, in direct proportion to

the decrease in the number of Δ_1 valleys constituting the conduction-band edge. The valence-band effective density of states N_v decreases from its bulk value with an increase of strain. This is due primarily to the splitting of the light and heavy holes, with the band edge being characterized by the low-effective-mass light hole ($m_j = \pm\frac{1}{2}$). The intrinsic carrier concentration mirrors the variation in band gap, being minimal in the strained film at the Δ_1-L_1 conduction-band-edge crossover, where the band gap is largest.

The data for the $Si_{0.5}Ge_{0.5}(001)$ substrate are shown in Fig. 6. Epitaxy of $Si_{1-x}Ge_x$ on a $Si_{0.5}Ge_{0.5}(001)$ substrate will result in either biaxial tensile ($x<0.5$) or compressive ($x>0.5$) strain. The conduction-band shifts are qualitatively as in the previous two cases of tensile (Ge substrate) and compressive (Si substrate) strain. The position of the Δ_1-L_1 conduction-band-edge crossover is shifted from 85% Ge to nearly 100% Ge. For $x<0.5$ (biaxial tensile strain), the valence-band edge is characterized by a strain-dependent combination of $|\frac{3}{2},\pm\frac{1}{2}\rangle$ and $|\frac{1}{2},\pm\frac{1}{2}\rangle$ states. For $x>0.5$ (biaxial compressive strain), the valence-band edge is characterized by $|\frac{3}{2},\pm\frac{3}{2}\rangle$ states. The shift in position of the Δ_1-L_1 conduction-band-edge crossover accounts for the rise in N_c near $x=1.0$. Away from $x=0.5$, N_c is seen to rapidly decrease as the conduction-band-edge degeneracies of the Δ_1 valleys are reduced. For both compressive and tensile strain, n_i is seen to generally increase above its bulk value. The exception to this occurs at $x \geq 0.9$. Here the strained-material conduction-band edge is characterized by the [100] and [010] valleys at a larger band gap than that of the four L_1 valleys at the band edge in the bulk. Since the band gap here is larger than that of the bulk, n_i falls below its bulk value.

The data for the Si(111) substrate are shown in Fig. 7. Primarily, the difference from Si(001) arising from this

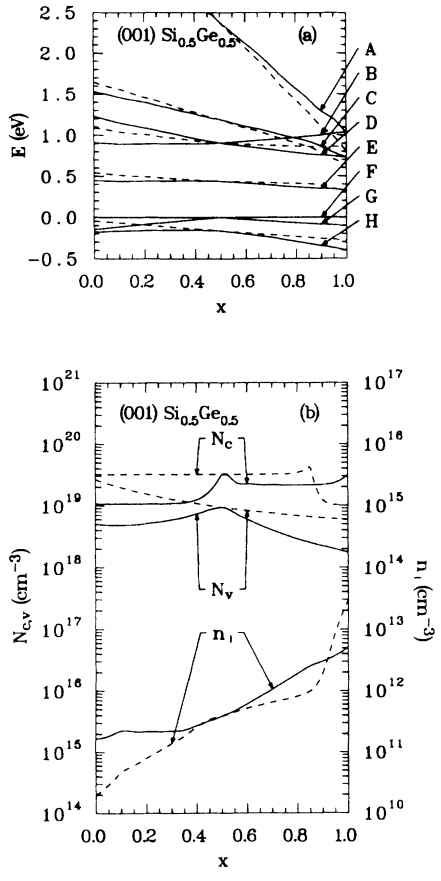

FIG. 6. $Si_{1-x}Ge_x/Si_{0.5}Ge_{0.5}(001)$. (a) Band-structure shifts as a function of Ge mole fraction x. Solid lines, energy levels in strained alloy film; dashed lines, energy levels in bulk alloy. *A*, [000] valley, conduction band; *B*, [001] valley, conduction band; *C*, [111], [11$\bar{1}$], [1$\bar{1}$1], and [$\bar{1}$11] valleys, conduction band; *D*, [100] and [010] valleys, conduction band; *E*, Fermi energy; *F*, valence-band edge (E_1); *G*, valence-band level E_2; *H*, valence-band level E_3. (b) Band-edge effective densities of state, N_c and N_v, and intrinsic carrier concentration n_i, as a function of Ge mole fraction x. Solid lines, values in strained alloy film; dashed lines, values in bulk alloy.

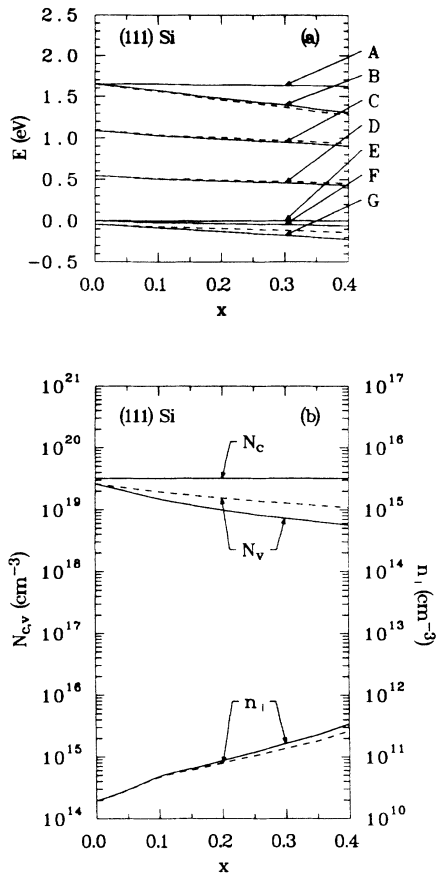

FIG. 7. $Si_{1-x}Ge_x/Si(111)$. (a) Band-structure shifts as a function of Ge mole fraction x. Solid lines, energy levels in strained alloy film; dashed lines, energy levels in bulk alloy. *A*, [111] valley, conduction band; *B*, [11$\bar{1}$], [1$\bar{1}$1], and [$\bar{1}$11] valleys, conduction band; *C*, [100], [010], and [001] valleys, conduction band; *D*, Fermi energy; *E*, valence-band edge (E_1); *F*, valence-band level E_2; *G*, valence-band level E_3. (b) Band-edge effective densities of state, N_c and N_v, and intrinsic carrier concentration n_i, as a function of Ge mole fraction x. Solid lines, values in strained alloy film; dashed lines, values in bulk alloy.

substrate orientation is that the L_1 conduction-band valleys are split, while the Δ_1 valleys are not. The [111] valley (A), whose wave vector is perpendicular to the substrate, rises above the other three L_1 valleys (B). The conduction-band edge is characterized by the Δ_1 valleys (C), which are shifted only slightly downward in energy. The valence band is the same in character as in the case of the Si(001) substrate, with the valence-band edge being characterized by the heavy-hole states (E). The light hole (F) and split-off hole (G) descend in energy with increasing strain. Because the primary strain-induced splitting, in the conduction band, does not involve states at the conduction-band edge [in distinction to the case of Si(001)], there is very little effect on N_c and n_i. The intrinsic carrier concentration increases only slightly above its bulk value, reflecting the only slight decrease in band gap. With increasing strain, the valence-band-edge effective density of states N_v is seen to decrease for the same reasons as in the case of the Si(001) substrate.

The data for the Ge(111) substrate are shown in Fig. 8. The most prominent feature of the band structure of $Si_{1-x}Ge_x$ grown on Ge(111) is that the conduction-band edge is characterized by the single [111] valley (D), whose wave vector is perpendicular to the substrate. The other significant conduction-band levels remain near their bulk positions, while the valence band is qualitatively the same as in the case of the Ge(001) substrate. The valence-band edge is characterized by the light hole (F). A single L_1 valley at the conduction-band edge leads to the great reduction in N_c, which actually drops below N_v in the strained film for $x<0.95$. The intrinsic carrier concentration increases slightly with strain, due to the decrease in band gap. However, this increase is not as great as in earlier cases, since the conduction-band edge has such a low density of states.

The data for the $Si_{0.5}Ge_{0.5}(111)$ substrate are shown in Fig. 9. Alloy growth on $Si_{0.5}Ge_{0.5}(111)$ leads to a band

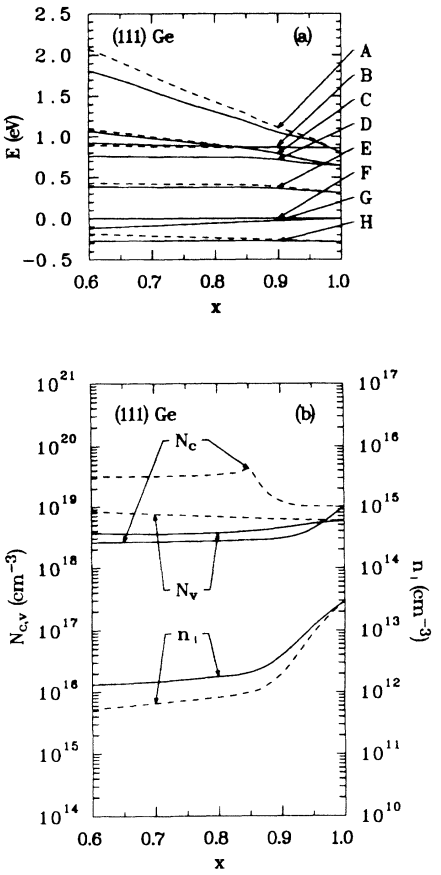

FIG. 8. $Si_{1-x}Ge_x/Ge(111)$. (a) Band-structure shifts as a function of Ge mole fraction x. Solid lines, energy levels in strained alloy film; dashed lines, energy levels in bulk alloy. A, [000] valley, conduction band; B, [100], [010], and [001] valleys, conduction band; C, [11$\bar{1}$], [1$\bar{1}$1], and [$\bar{1}$11] valleys, conduction band; D, [111] valley, conduction band; E, Fermi energy; F, valence-band edge (E_1); G, valence-band level E_2. H, valence-band level E_3. (b) Band-edge effective densities of state, N_c and N_v, and intrinsic carrier concentration n_i, as a function of Ge mole fraction x. Solid lines, values in strained alloy film; dashed lines, values in bulk alloy.

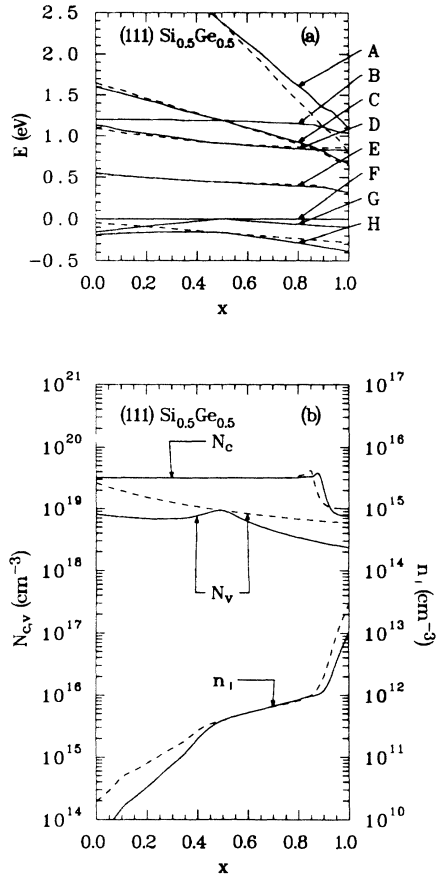

FIG. 9. $Si_{1-x}Ge_x/Si_{0.5}Ge_{0.5}(111)$. (a) Band-structure shifts as a function of Ge mole fraction x. Solid lines, energy levels in strained alloy film; dashed lines, energy levels in bulk alloy. A, [000] valley, conduction band; B, [111] valley, conduction band; C, [11$\bar{1}$], [1$\bar{1}$1], and [$\bar{1}$11] valleys, conduction band; D, [100], [010], and [001] valleys, conduction band; E, Fermi energy; F, valence-band edge (E_1); G, valence-band level E_2; H, valence-band level E_3. (b) Band-edge effective densities of state, N_c and N_v, and intrinsic carrier concentration n_i, as a function of Ge mole fraction x. Solid lines, values in strained alloy film; dashed lines, values in bulk alloy.

structure which in most respects is similar to that of the bulk. However, the splitting of the L_1 valleys causes a reduction in the number of L_1 valleys at the band edge, above the Δ_1-L_1 conduction-band-edge crossover. Only the [11$\bar{1}$], [1$\bar{1}$1], and [$\bar{1}$11] valleys (C) constitute the conduction-band edge at an energy slightly higher than in the bulk. This slight increase in band gap results in a slight decrease in n_i, above crossover. The valence band has the same qualitative character as in the case of the $Si_{0.5}Ge_{0.5}$(001) substrate. It should be pointed out that in distinction to the case of the $Si_{0.5}Ge_{0.5}$(001) substrate, growth on the (111) orientation retains the Δ_1-L_1 conduction-band-edge crossover near its position in the bulk. This means that the value of N_c will be similar between the strained and bulk material. The valence-band effective density of states decreases with increasing strain as in the case of the $Si_{0.5}Ge_{0.5}$(001) substrate. The intrinsic carrier concentration decreases with strain due to both a slight increase in band gap and the decrease in N_v.

The data for the Si(101) substrate are shown in Fig. 10. Growth on a Si(101) substrate results in splittings of both the L_1 and Δ_1 conduction-band valleys. The [111] and [1$\bar{1}$1] valleys (A) rise above the [11$\bar{1}$] and [$\bar{1}$11] valleys (B) under the biaxial compressive strain. The [100] and [001] valleys (C) rise above the [010] valley (D), which constitutes the conduction-band edge. The valence-band edge is characterized by eigenstates composed primarily of $|\frac{3}{2},\pm\frac{3}{2}\rangle$ states with a lesser amount of $|\frac{3}{2},\pm\frac{1}{2}\rangle$ and $|\frac{1}{2},\pm\frac{1}{2}\rangle$. There is a greater decrease in N_c with strain than in the case of the Si(001) substrate because only one-third of the Δ_1 states (only [010]) compose the conduction-band edge (compared to two-thirds, [100] and [010], for the Si(001) substrate). However, the splitting of the Δ_1 valleys with strain is more gradual than in

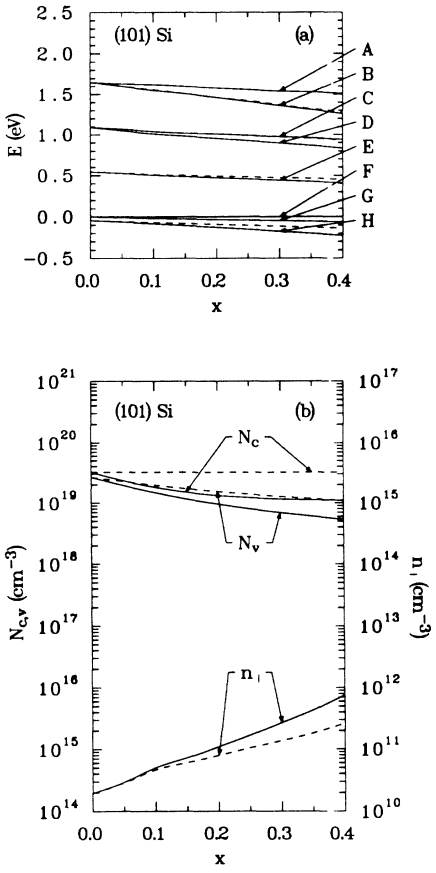

FIG. 10. $Si_{1-x}Ge_x$/Si(101). (a) Band-structure shifts as a function of Ge mole fraction x. Solid lines, energy levels in strained alloy film; dashed lines, energy levels in bulk alloy. A, [111] and [1$\bar{1}$1] valleys, conduction band; B, [11$\bar{1}$] and [$\bar{1}$11] valley, conduction band; C, [100] and [001] valleys, conduction band; D, [010] valley, conduction band; E, Fermi energy; F, valence-band edge (E_1); G, valence-band level E_2; H, valence-band level E_3. (b) Band-edge effective densities of state, N_c and N_v, and intrinsic carrier concentration n_i, as a function of Ge mole fraction x. Solid lines, values in strained alloy film; dashed lines, values in bulk alloy.

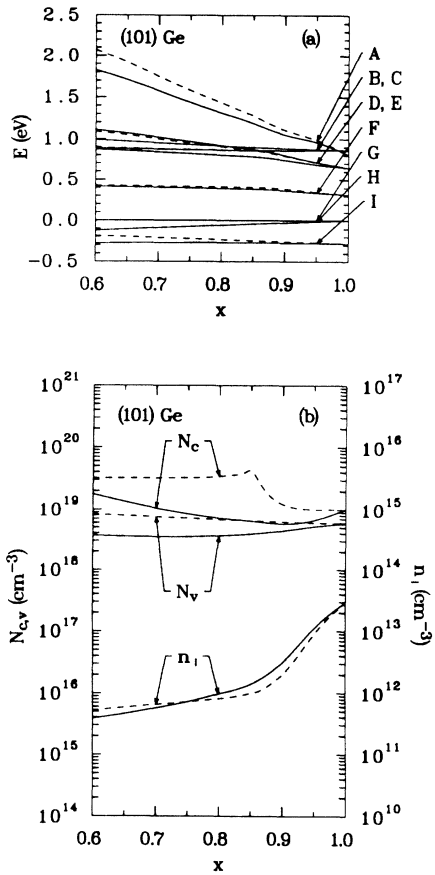

FIG. 11. $Si_{1-x}Ge_x$/Ge(101). (a) Band-structure shifts as a function of Ge mole fraction x. Solid lines, energy levels in strained alloy film; dashed lines, energy levels in bulk alloy. A, [000] valley, conduction band; B, [010] valley, conduction band; C, [100] and [001] valleys, conduction band ([100] and [001] valleys are below [010] valley in energy); D, [11$\bar{1}$] and [$\bar{1}$11] valleys, conduction band; E, [111] and [1$\bar{1}$1] valleys, conduction band ([111] and [1$\bar{1}$1] valleys are below [11$\bar{1}$] and [$\bar{1}$11] valleys in energy); F, Fermi energy; G, valence-band edge (E_1); H, valence-band level E_2; I, valence-band level E_3. (b) Band-edge effective densities of state, N_c and N_v, and intrinsic carrier concentration n_i, as a function of Ge mole fraction x. Solid lines, values in strained alloy film; dashed lines, values in bulk alloy.

previous cases. This leads to the decrease in N_c being spread out over a wider range of x.

The data for the Ge(101) substrate are shown in Fig. 11. Here no Δ_1-L_1 conduction-band-edge crossover is found for the displayed range of x. The conduction-band edge is characterized by the [111] and [1$\bar{1}$1] valleys (E), which are split from the [11$\bar{1}$] and [$\bar{1}$11] valleys (D). The Δ_1 valleys split, with the [100] and [001] valleys (C) lying below the [010] valley (B). The valence-band edge is characterized by eigenstates composed primarily of $|\frac{3}{2},\pm\frac{1}{2}\rangle$ and $|\frac{1}{2},\pm\frac{1}{2}\rangle$ states, with a lesser amount of $|\frac{3}{2},\pm\frac{3}{2}\rangle$. The strain-induced splitting of the conduction-band-edge valleys leads to the observed reduction in N_c. Since no Δ_1-L_1 conduction-band-edge crossover occurs, the peaks in N_c, present in bulk, is absent in the strained material.

The data for the $Si_{0.5}Ge_{0.5}$(101) substrate are shown in Fig. 12. Here, as in the other cases of the (101) substrate, both the L_1 and Δ_1 valleys are split by the strain. In Fig. 12(a), curves labeled B and E are the [111], [1$\bar{1}$1] valleys and [11$\bar{1}$],[$\bar{1}$11] valleys, respectively. Curves C and D are the [100],[001] valleys and the [010] valley, respectively. The position of the Δ_1-L_1 conduction-band-edge crossover shifts to approximately 89% Ge. For $x<0.5$, the conduction-band edge is characterized by the [010] Δ_1 valley. Between $x=0.5$ and 0.89, the conduction-band edge consists of the [100] and [001] valleys. Above $x=0.89$, the [11$\bar{1}$] and [$\bar{1}$11] valleys form the conduction-band edge. Below $x=0.5$ (biaxial tensile strain), the valence-band edge eigenstates are dominantly $m_j=\pm\frac{1}{2}$ with a slight amount of $m_j=\pm\frac{3}{2}$ states. Above $x=0.5$ (biaxial compressive strain), the valence-band-edge eigenstates switch and become dominantly $m_j=\pm\frac{3}{2}$ with a slight amount of $m_j=\pm\frac{1}{2}$. The band-edge effective densities of states exhibit the same qualitative features found in other substrates. For $x<0.5$, the intrinsic carrier concentration n_i lies below its bulk value. This is because the band gap is very close to the bulk band gap, while N_c and N_v are decreased.

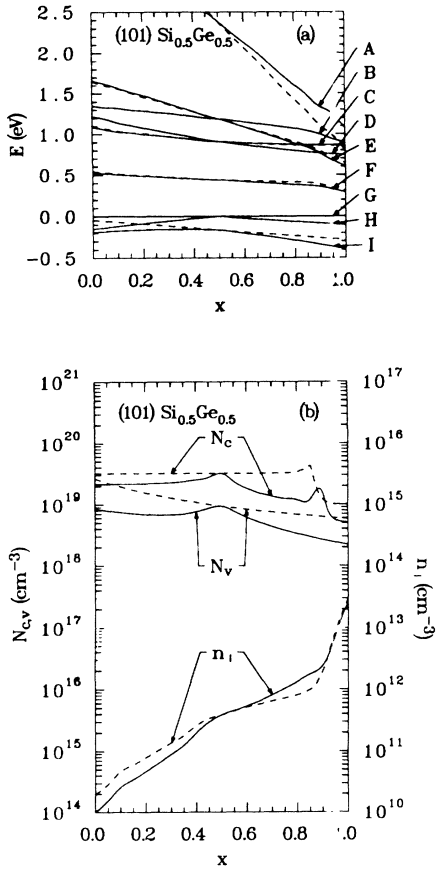

FIG. 12. $Si_{1-x}Ge_x/Si_{0.5}Ge_{0.5}$(101). (a) Band-structure shifts as a function of Ge mole fraction x. Solid lines, energy levels in strained alloy film; dashed lines, energy levels in bulk alloy. A, [000] valley, conduction band; B, [111] and [1$\bar{1}$1] valleys, conduction band; C, [100] and [001] valleys, conduction band; D, [010] valleys, conduction band; E, [11$\bar{1}$] and [1$\bar{1}$1] valleys, conduction band; F, Fermi energy; G, valence-band edge (E_1); H, valence-band level E_2; I, valence-band level E_3. (b) Band-edge effective densities of state, N_c and N_v, and intrinsic carrier concentration n_i, as a function of Ge mole fraction x. Solid lines, values in strained alloy film; dashed lines, values in bulk alloy.

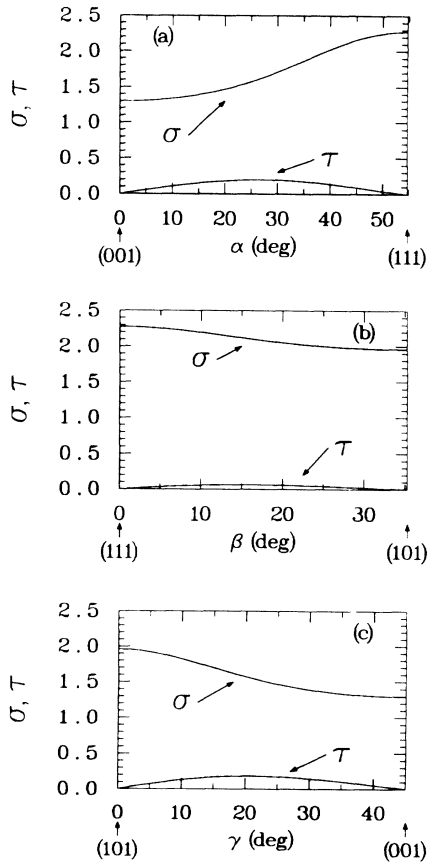

FIG. 13. Poisson's ratio σ and shear parameter τ variation with substrate orientation. (a) From (001) to (111), the angle between [001] and [111] is $\alpha_{max}=54.736°$; (b) from (111) to (101), the angle between [111] and [101] is $\beta_{max}=35.264°$; (c) from (101) to (001), the angle between [101] and [001] is $\gamma_{max}=45°$.

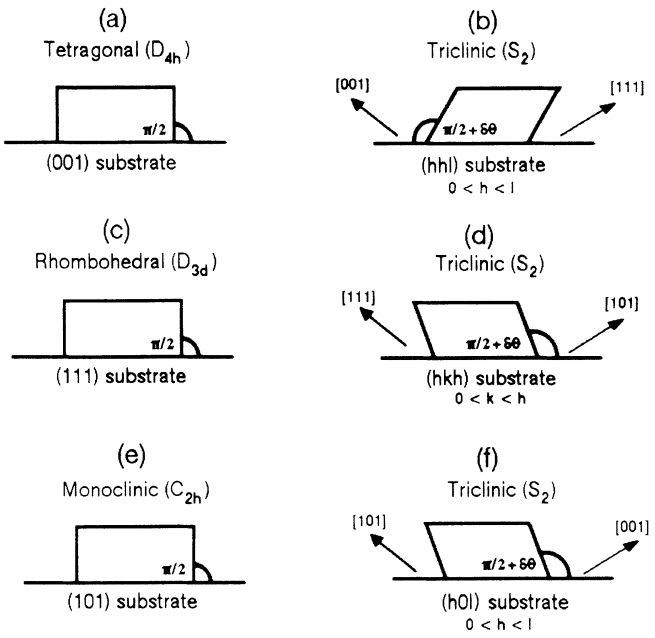

FIG. 14. Schematic edge view of distortion of film lattice due to epitaxy on various substrate orientations. Figures are shown for $\varepsilon_{\parallel} > 0$. For (001), (111), and (101) substrates, the distortion is a combination of a hydrostatic compression or dilation and a uniaxial extension or contraction perpendicular to the substrate surface [(a), (c), and (e)]. For other substrate orientations between these [(b), (d), and (f)], the distortion exhibits an additional shear, relative to the plane of the substrate. The sense of inclination reverses for a biaxial compressive strain ($\varepsilon_{\parallel} < 0$). The amount of inclination, as shown, is $\delta\theta = 2\tau\varepsilon_{\parallel}$.

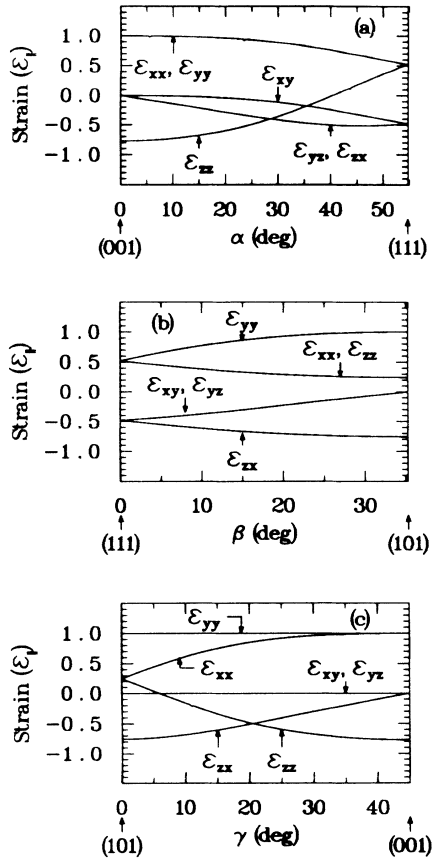

FIG. 15. Strain-tensor-component variation with substrate orientation. Components are plotted in units of $\varepsilon_{\parallel}$. (a) From (001) to (111), the angle between [001] and [111] is $\alpha_{max} = 54.736°$; (b) from (111) to (101), the angle between [111] and [101] is $\beta_{max} = 35.264°$; (c) from (101) to (001), the angle between [101] and [001] is $\gamma_{max} = 45°$.

VI. CONCLUSION

Poisson's ratio σ and $\varepsilon_{\parallel}$ are sufficient to determine the strain tensor in films on (001), (111), and (101) substrates. However, as discussed in the Appendix, an additional shear, quantified by the parameter τ, appears in films grown on substrates of any other orientation. Many features of the band structure can be controlled by judicious choice of substrate composition and crystallographic orientation. The direction of shift of a given conduction-band valley under strain deformation is found to depend not only on the sense of the in-plane lattice mismatch strain $\varepsilon_{\parallel}$, but also upon the substrate orientation. The Δ_1-L_1 conduction-band-edge crossover point can be shifted in either direction, away from its bulk position of 85% Ge, in high-Ge-content alloys. The intrinsic carrier concentration n_i is found to be primarily controlled by the value of the band gap, varying inversely with E_g. Only when the conduction-band edge is characterized by a very low density of states, under strain-induced valley splitting, does the value of n_i not increase strongly with decreasing band gap. An example of this is the case of the Ge(111) substrate, where only one of the L_1 valleys constitutes the conduction-band edge. Generally, the intrinsic Fermi energy E_i is found to remain near the middle of the band gap, being only slightly affected by the values of N_c and N_v. The conduction- and valence-band-edge effective densities of state are found to generally decrease as the degree of strain, either compressive or tensile, increases. An exception to this is in the case of a high-Ge-content alloy under biaxial compression. The lowering of some or all of the Δ_1 valleys under such strain may lead to an increase in N_c. Generally, the splitting of the valleys which constitute the conduction-band edge and the lifting of the valence-band-edge degeneracies both contribute to decreases in N_c and N_v. The further factor contributing to the decrease in N_v is the increase of the valence-band curvature with strain. This may be seen as a reduction in the valence-band effective mass.

The Si-Ge alloy system is already promising remarkable improvements in high-speed Si technology compatible electronic devices. It is natural to expect that other heterostructures based on the Si-Ge system will be exploited. Our studies show that a tremendous richness in band tailoring effects can be accessed by developing an understanding of the physics of pseudomorphic films.

ACKNOWLEDGMENTS

This work was supported by the U.S. Army Research Office (Grant No. DAAL03-87-K-0007), and by a grant from the IBM Corporation (Armonk, NY).

APPENDIX

The general derivation of the strain tensor in an epitaxial film is presented here. The special cases of films grown on substrates of the (001), (111), and (101) crystallographic orientations were developed in Sec. II. These cases were special in that the substrate normal is an axis of n-fold rotational symmetry ($n \geq 2$) for the epitaxial film. These substrates are most frequently of interest. However, occasionally other substrates, such as (112), appear in the literature. Also, substrates which are a few degrees misaligned from (001) are not uncommon. In light of the possibility of using these sorts of substrates in pseudomorphic heteroepitaxy, the determination of the film's strain tensor becomes important as the starting point for a theoretical analysis of the system.

The determination of the strain tensor is taken up from Eq. (5) of Sec. II, which repeated here, is

$$C'_{\alpha\beta ij}\varepsilon'_{ij}=0, \quad (\alpha,\beta)=(1,3),(2,3),(3,3) , \tag{A1}$$

with summation over repeated indices. For $(i,j)=(1,1),(2,2),(1,2),(2,1)$, ε'_{ij} is known: $\varepsilon'_{11}=\varepsilon'_{22}=\varepsilon_{\parallel}$, $\varepsilon'_{12}=\varepsilon'_{21}=0$. Using the symmetry of $C'_{\alpha\beta ij}$ and ε'_{ij},

$$C'_{\alpha\beta 33}\varepsilon'_{33}+2C'_{\alpha\beta 23}\varepsilon'_{23}+2C'_{\alpha\beta 31}\varepsilon'_{31}=-(C'_{\alpha\beta 11}+C'_{\alpha\beta 22})\varepsilon_{\parallel} ,$$
$$(\alpha,\beta)=(3,3),(2,3),(1,3) . \tag{A2}$$

This may be written as a matrix equation:

$$\begin{bmatrix} C'_{3333} & C'_{3323} & C'_{3331} \\ C'_{2333} & C'_{2323} & C'_{2331} \\ C'_{3133} & C'_{3123} & C'_{3131} \end{bmatrix} \begin{bmatrix} \varepsilon'_{33}/2 \\ \varepsilon'_{23} \\ \varepsilon'_{31} \end{bmatrix} = -\frac{\varepsilon_{\parallel}}{2} \begin{bmatrix} C'_{3311}+C'_{3322} \\ C'_{2311}+C'_{2322} \\ C'_{3111}+C'_{3122} \end{bmatrix} . \tag{A3}$$

The $C'_{\delta\gamma kl}$ matrix elements are determined from $C_{\alpha\beta ij}$ via Eq. (3), Sec. II. Trigonometric identities are used to arrive at the simple form

$$\begin{aligned} C'_{\gamma\delta kl} = & c_{11}\sum_{\alpha=1}^{3} U_{\alpha\gamma}U_{\alpha\delta}U_{\alpha k}U_{\alpha l} \\ & + c_{12}\sum_{\beta=2}^{3}\sum_{\alpha=1}^{\beta-1}(U_{\alpha\gamma}U_{\alpha\delta}U_{\beta k}U_{\beta l}+U_{\beta\gamma}U_{\beta\delta}U_{\alpha k}U_{\alpha l}) \\ & + c_{44}\sum_{\beta=2}^{3}\sum_{\alpha=1}^{\beta-1}(U_{\alpha\gamma}U_{\beta\delta}+U_{\beta\gamma}U_{\alpha\delta}) \\ & \times(U_{\alpha k}U_{\beta l}+U_{\beta k}U_{\alpha l}) , \end{aligned} \tag{A4}$$

where the U_{ij} are elements of the transformation matrix $\underline{U}$ [Eq. (2), Sec. II]. Having calculated the various elements $C'_{\delta\gamma kl}$, Eq. (A3) can be inverted numerically to determine ε'_{33}, ε'_{23}, and ε'_{31}.

Knowing ε'_{33} in terms of $\varepsilon_{\parallel}$, Poisson's ratio σ is straightforwardly obtained: $\sigma=-\varepsilon_{\parallel}/\varepsilon'_{33}$. However, in the case of the arbitrarily oriented substrate, σ and $\varepsilon_{\parallel}$ are not sufficient to completely specify the strain in the film, since ε'_{23} and ε'_{31} are generally nonzero. The strain components ε'_{23} and ε'_{31} may be characterized by (1) the angle ψ through which a rotation, about z', from (x',y',z') to (x'',y'',z') will result in $\varepsilon''_{23}=0$ and by (2) by ratio $\tau\equiv\varepsilon''_{31}/|\varepsilon_{\parallel}|$. It may easily be determined that

$$\tan\psi=-\frac{\varepsilon'_{23}}{\varepsilon'_{13}} ,$$
$$\tau=\frac{[(\varepsilon'_{31})^2+(\varepsilon'_{23})^2]^{1/2}}{|\varepsilon_{\parallel}|} . \tag{A5}$$

The parameter τ is similar in character to Poisson's ratio σ. If the strained film is viewed from the edge, Poisson's ratio expresses the degree to which geometrical squares fixed to the lattice are deformed to rectangles as the film is strained. The parameter τ expresses the degree to which the squares are deformed to rhombohedra.

Both σ and τ are plotted as functions of substrate orientation in Fig. 13. At the points corresponding to (001), (111), and (101) orientations, τ is seen to equal zero, as expected. In these orientations the film distortion is characterized by Poisson's ratio only and thus can be viewed as tetragonally distorted (squares become rectangles) relative to the plane of the substrate. For (hhl) substrates oriented between the (001) and (111) directions, the film inclines under shear distortion toward the (111) direction by the angle $\delta\theta=2\tau\varepsilon_{\parallel}$. In (hkh) substrates oriented between (111) and (101), the tilt is toward [111], by $\delta\theta$, and in $(h0l)$ substrates, between (101) and (001), the tilt is toward [101], by $\delta\theta$. Of course, when $\varepsilon_{\parallel}<0$, the tilting is away from the above stated directions, by $\delta\theta$. This is clarified in Fig. 14. The strain tensor components, relative to the standard coordinates, (x,y,z) of the crystallographic axes of the film are plotted in Fig. 15. This plot shows the dependence of the strain tensor components on substrate orientation, as the orientation is varied from (001) to (111) to (101) and back to (001). These data are obtained by solving Eq. (A3) for ε'_{33}, ε'_{23}, and ε'_{31}. These elements, together with the known elements ε'_{11}, ε'_{22}, and ε'_{12}, are inverted [Eq. (18), Sec. II] to give the data shown in Fig. 15.

[1]R. People, IEEE J. Quantum Electron. **QE-22**, 1696 (1986).

[2]K. Godwod, R. Kowalczyk, and Z. Szmid, Phys. Status Solidi A **21**, 227 (1974).

[3]J. F. C. Baker and M. Hart, Acta Crystallogr. Sect. A **31**, 364 (1975).

[4]H. J. McSkimin and P. Andreatch, J. Appl. Phys. **35**, 2161 (1964).

[5]J. S. Kline, F. H. Pollak, and M. Cardona, Helv. Phys. Acta **41**,

968 (1968).
[6]S. Zwerdling, B. Lax, L. M. Roth, and K. J. Button, Phys. Rev. **114**, 80 (1959).
[7]B. Welber, C. K. Kim, M. Cardona, and S. Rodriguez, Solid State Commun. **17**, 1021 (1975).
[8]R. Braunstein, A. R. Moore, and F. Herman, Phys. Rev. **109**, 695 (1958).
[9]R. A. Forman, W. R. Thurber, and D. E. Aspnes, Solid State Commun. **14**, 1007 (1974).
[10]F. H. Pollak and M. Cardona, Phys. Rev. **172**, 816 (1968).
[11]A. Jayaraman, B. B. Kosicki, and J. C. Irvin, Phys. Rev. **171**, 836 (1968).
[12]I. Balslev, Phys. Rev. **143**, 636 (1966).
[13]I. Balslev, Phys. Lett. **24A**, 113 (1967).
[14]E. Burstein, G. S. Picus, R. F. Wallis, and F. Blatt, Phys. Rev. **113**, 15 (1959).
[15]H. D. Barber, Solid State Commun. **10**, 1039 (1967).
[16]D. Fink and R. Braunstein, Phys. Status Solidi B **73**, 361 (1976).
[17]S. Zwerdling, K. J. Button, B. Lax, and L. M. Roth, Phys. Rev. Lett. **4**, 173 (1960).
[18]S. H. Groves, C. R. Pidgeon, and J. Feinleib, Phys. Rev. Lett. **17**, 643 (1966).
[19]P. Lawaetz, Phys. Rev. B **4**, 3460 (1971).
[20]J. D. Wiley, Solid State Commun. **8**, 1865 (1970).
[21]D. Geist and F. Balck, Phys. Status Solidi B **56**, 557 (1973).
[22]G. Dresselhaus, A. F. Kip, and C. Kittel, Phys. Rev. **98**, 368 (1955).
[23]M. Tiersten, IBM J. Res. Dev. **5**, 122 (1961).
[24]E. Otsuka, S. Nagata, and K. Murase, J. Phys. Soc. Jpn. **20**, 727 (1965).
[25]G. Dresselhaus, A. F. Kip, H.-Y. Ku, G. Wagoner, and S. M. Christian, Phys. Rev. **100**, 1218 (1955).
[26]R. Braunstein, Phys. Rev. **130**, 869 (1963).
[27]G. L. Bir and G. E. Pikus, *Symmetry and Strain Induced Effects in Semiconductors* (Wiley, New York, 1974).
[28]G. E. Pikus and G. L. Bir, Fiz. Tverd. Tela (Leningrad) **1**, 1642 (1959) [Sov. Phys.—Solid State **1**, 1502 (1959)].
[29]R. P. Feynman, R. B. Leighton, and M. Sands, *The Feynman Lectures on Physics* (Addison-Wesley, Reading, MA, 1965), Vol. 3.